A Genome-Wide Genetic Screen Identifies a Novel kDNA Replication Protein in Trypanosomes

Migla Miskinyte,[a*] Clirim Jetishi,[b] Ana Kalichava,[b*] Alasdair Ivens,[a] Martin Waterfall,[a] , Matt Gould,[a] Lucy Glover,[c*] David Horn,[c] Torsten Ochsenreiter,[b] Achim Schnaufer[a#]

[a]Institute of Immunology and Infection Research, University of Edinburgh, UK

[b]Institute of Cell Biology, Faculty of Science, University of Bern, Switzerland

[c]Wellcome Centre for Anti-Infectives Research, School of Life Sciences, University of Dundee, UK.

Running Head: A novel trypanosome kDNA replication factor

#Address correspondence to Achim Schnaufer, achim.schnaufer@ed.ac.uk

*Present address:

Migla Miskinyte, Ophiomics, Lisbon, Portugal

Ana Kalichava, Artidis, Basel, Switzerland

Lucy Glover, Institut Pasteur, Paris, France

Word count abstract: 250

Word count text (exclusive of references, tables, and figure legends): 6912

ABSTRACT

Trypanosomatid parasites cause diverse diseases in humans and their livestock, but share a unique biological feature, the organization of mitochondrial DNA into a complex structure, named kinetoplast (kDNA), which is crucial for the survival of the parasites. Replication, segregation and expression of kDNA are highly complex processes that involve an estimated ~300 proteins, only a fraction of which have been identified and characterized. Here, we report the development of an unbiased genetic screen in the experimental model *Trypanosoma brucei* to identify novel factors involved in kDNA maintenance. Our approach uses a combination of genome-wide RNA interference, a novel kDNA staining protocol, and fluorescence-activated cell sorting. Of the 20 highest-ranked genes identified, six are known kDNA maintenance factors. One hit, *Tb927.8.4240*, a gene of previously unknown function, was selected for experimental validation and follow-up. Ultrastructure expansion microscopy using a tagged version of the protein reveals a dynamic localization during the cell cycle. RNAi-mediated ablation of *Tb927.8.4240* results in the progressive but incomplete loss of kDNA, with only a minor effect on the tripartite attachment complex, suggesting the protein is involved in kDNA replication but not segregation. The growth phenotype of *Tb927.8.4240* ablation is fully rescued in a kDNA-independent genetic background, confirming a specific role in kDNA replication.

In summary, we describe a functional genetic screen for the identification of kDNA maintenance factors in trypanosomes, validate one hit as a novel kDNA replication factor, and provide a prioritized hit list as a promising starting point for the future identification of additional factors.

43 **IMPORTANCE**

44 Trypanosomatid parasites cause several important diseases in humans and their livestock, such as
45 sleeping sickness, leishmaniasis, Chagas disease and nagana. Critical for survival of these
46 parasites in their hosts and vectors is faithful maintenance and expression of their mitochondrial
47 DNA, called kinetoplast DNA (or kDNA). Indeed, several established anti-trypanosomal drugs
48 interfere with these processes. Kinetoplast DNA maintenance is an extraordinarily complex
49 process and incompletely understood. Here we describe the development of a functional genetic
50 screen in the parasite *Trypanosoma brucei* for the identification of genes that are important for
51 kDNA maintenance. The top 20 screening hits include six known kDNA maintenance genes,
52 which validates this screen. Using gene knockdown by RNA interference and localization studies
53 with ultrastructure expansion microscopy we characterize one hit, a gene with the systematic
54 identifier *Tb927.8.4240*, as a novel kDNA replication factor. The hit list from this screen
55 provides a useful resource for future research.

56

57 **INTRODUCTION**

58 Kinetoplastids are a group of flagellated protists that include the important human and animal
59 pathogens of the genera *Trypanosoma* and *Leishmania* (1). A hallmark feature of these
60 organisms is the kinetoplast DNA (kDNA), the organellar DNA within their single
61 mitochondrion (2). Like mitochondrial DNA of other eukaryotes, kDNA encodes subunits of the
62 mitochondrial oxidative phosphorylation (OXPHOS) system and the mitoribosome (3–5).
63 However, unlike typical mitochondrial DNA, kDNA is arranged in a massive, catenated network
64 comprising 5,000 – 10,000 minicircles and dozens of maxicircles, all physically linked into a
65 planar disk (2, 6). The kDNA disk itself is physically linked to the flagellum's basal body by the
66 so called tripartite attachment complex (TAC), a fibrous structure that crosses both
67 mitochondrial membranes (7). The intricate kDNA network is not only visually striking when
68 observed with electron or atomic force microscopy (8, 9) but is also essential for the survival and
69 propagation of trypanosomes, as the encoded genes are critical for mitochondrial function and
70 parasite viability (2, 5, 6, 10).

71 The complexity of the kDNA structure is functionally linked to equally complex mechanisms
72 for mitochondrial gene expression. Out of the 18 mRNAs encoded in the maxicircles (20–30 kb
73 in length in *T. brucei*), 12 require post-transcriptional editing by insertion and removal of
74 uridines (11). For some mRNAs this editing is extensive and results in more than doubling of the
75 mRNA length. The precise number of uridines to be inserted or removed, and the location of
76 editing events within the mRNAs, is specified by short guide RNAs (gRNAs) by virtue of their
77 complementarity to the fully edited sequence. The vast majority of gRNAs are encoded by
78 minicircles (~1 kb in length in *T. brucei*, with 3-4 gRNA genes per minicircle (12)). Hence, the
79 sequence information for most kDNA-encoded genes is split between maxicircles and

80 minicircles, and faithful replication and transfer to daughter cells of both types of molecules
81 during cell division is therefore critical for parasite viability. Indeed, interference with kDNA
82 maintenance is a key part of the mode of action of several anti-trypanosomatid drugs (13, 14).

83 Unsurprisingly, elucidation of the precise mechanism of kDNA replication and segregation,
84 and of the molecular machineries responsible for these processes, has been a major focus of
85 research, and the current state of knowledge of these processes has been detailed in several
86 reviews (e.g. (2, 15, 16)). Replication and segregation of kDNA are highly regulated, multi-
87 phase processes that occur once per cell cycle and involve the orchestrated action of numerous
88 enzymatic and structural proteins and complexes. Summarised briefly, replication initiates with
89 the release of individual minicircles from the kDNA network (presumably by topoisomerase 2)
90 into the so-called kinetoflagellar zone (KFZ) between kDNA disk and inner mitochondrial
91 membrane, where they undergo unidirectional theta-type replication (17). The process probably
92 involves DNA polymerase IB and universal minicircle binding protein 1 (18, 19). The resulting
93 daughter minicircles are then reattached to the network at so-called antipodal sites (APS) at
94 opposite sides of the network periphery, a process that must require precise topological control to
95 prevent entanglement and ensure network integrity (16). The APS are still poorly defined in
96 composition and structure, but have been reported to contain several components of the kDNA
97 replication machinery, including enzymes required for reattachment of minicircles into the
98 network (topoisomerase 2 (20), possibly MiRF172 (21)), initiation of replication (primase 2
99 (22)), primer removal (helicases PIF1 and PIF5 (23, 24)), and gap repair (polymerase β (25),
100 DNA ligase LigK-β (26)). The traditional model for minicircle replication postulates a sorting
101 mechanism that ensures the distribution of the two daughter minicircles to opposite APS (2).
102 More recently, reexamination of available localization data for kDNA replication factors led to

103 an alternative 'loose-diploid' model that envisions two distinct lobes within the kDNA disk, each
104 with an essentially complete set of minicircles that are released from the network laterally,
105 replicated and then reattached to the same lobe (27). In both models, maxicircles remain attached
106 to the network for replication (28), which likely involves DNA polymerases IC and ID (29, 30).

107 Following replication, the accurate segregation of the kDNA daughter networks into daughter
108 cells is facilitated by the TAC, which links this process to the duplication and segregation of the
109 basal body during cell division. The molecular architecture and biogenesis of the TAC has been
110 dissected in considerable detail in recent years (reviewed in (15, 16)). TAC consists of three
111 distinct subdomains: the extramitochondrial exclusion zone filaments (EZF) between the basal
112 body and the outer mitochondrial membrane, the intramitochondrial unilateral filaments (ULF)
113 between inner mitochondrial membrane and kDNA, and the differentiated membranes (DM) that
114 bridge EZF and ULF. The DM subdomain is complex and consists of at least four different
115 proteins (pATOM36, TAC40, TAC42 and TAC60; (15)). The EZF appears to consist of a single
116 component, p197, that directly binds the basal body and is linked to the DM via TAC65 (31).
117 The ULF consists of at least TAC53 (32), p166 (33) and TAC102 (34); the molecular details of
118 its interaction with the kDNA disk itself remains to be elucidated, but may involve at least two
119 additional proteins that are not part of the TAC itself (35).

120 Overall, 63 different proteins have to date been reported as 'kinetoplast-associated' (36),
121 which includes the kDNA replication factors and TAC components described above, and it was
122 estimated that kDNA repair, replication and segregation may involve around 150 proteins (8).
123 Important aspects of these processes that remain to be elucidated include the precise structural
124 organisation of kDNA replication, including the mechanism of transport of minicircle replication

125 intermediates to the reattachment sites, how topology and size of the network are controlled, and
126 how replication of kDNA and of nuclear DNA are coordinated and integrated into the cell cycle.

127 The impressive progress that has been made in identifying components of kDNA replication
128 and segregation in trypanosomes has resulted from a combination of bioinformatics, biochemical
129 and imaging approaches, with each providing complementary insights into the molecular and
130 cellular players and processes. In recent years, genome-wide RNAi screens in trypanosomes that
131 select for phenotypes of interest after gene ablation have become a powerful tool in trypanosome
132 research (37), but so far such screens have not been applied to the study of kDNA replication and
133 segregation. Here, we developed an unbiased genetic screen for loss of kDNA after ablation of
134 gene expression, aiming to identify novel factors that play critical roles in kDNA maintenance
135 and its regulation and to help fill some of the gaps in understanding outlined above.

136

137 # RESULTS

138 **Development of a whole-genome scale RNAi screen for kDNA loss**

139 We designed a screening approach based on a combination of genome-wide RNA interference, a
140 novel kDNA staining protocol, and fluorescence-activated cell sorting (FACS) of $kDNA^0$ cells;
141 an overview is presented in **Fig. S1**. A key tool in our screening approach is the ability to
142 genetically engineer bloodstream form *T. brucei* cells that are viable in the absence of kDNA
143 (38). This is achieved by expressing a mutated copy of the γ subunit (γL262P) of the
144 mitochondrial F_1F_O-ATPase, allowing for the creation of a mitochondrial membrane potential in
145 the absence of kDNA-encoded genes (38). We transfected these kDNA-independent *T. brucei*
146 cells with a whole-genome RNAi library (39, 40), achieving coverage of 60-87% for the eleven
147 megabase chromosomes, based on Illumina sequencing of RNAi inserts PCR-amplified from
148 transfected cells and mapping of reads to the *T. brucei* TREU927 reference genome (**Table S1**).
149 Another essential advancement was our development of an *in vivo* DNA staining protocol that
150 allowed the sorting, by flow cytometry, of trypanosome cells that had lost their kDNA. Initial
151 attempts using dihydroethidium (DHE), a dye previously reported to be specific for kDNA (42),
152 did not yield a sufficient separation of $kDNA^+$ and $kDNA^0$ cells by flow cytometry. However,
153 subsequent trials of co-staining with DHE and dsFLUOR (43) resulted in a clear, if imperfect,
154 separation of $kDNA^+$ and $kDNA^0$ *T. brucei* cells, as shown in **Fig. S1B**.

155 **Identification of putative kDNA maintenance factors**

156 In previous studies, RNAi-mediated ablation of kDNA maintenance factors in bloodstream form
157 parasites has been shown to result in kDNA loss after 3-5 days (35, 44). We therefore induced
158 RNAi in our library cells for 5 days, after which $kDNA^0$ cells were isolated by FACS (**Fig. S1A**).

159 After extraction of total DNA from the kDNA^0 cells, RNAi inserts were amplified by PCR (41)
160 and sequenced on an Illumina platform (100 bp pair-ended) using an amplification-free library
161 preparation protocol (sample 'Day 5 +tet kDNA^0'). For controls, we processed samples from (i)
162 the full RNAi cell library prior to induction ('Day 0') and (ii) from cells un-induced for 5 days
163 but sorted for kDNA^0 ('Day 5 -tet kDNA^0'). This strategy aimed to distinguish gene fragments
164 specifically enriched due to RNAi induction from those lost due to background noise or
165 nonspecific effects. Illumina reads were mapped to a *T. brucei* reference genome (45) and
166 differentially abundant reads per gene between tested conditions were determined.

167 **Fig. 1 panels A and B** show volcano plots, with thresholds for statistical significance set at
168 $\log_2$ fold-change > 1.5 and $p < 0.05$. These criteria identified 1852 and 436 candidate genes,
169 respectively, with an overlap of 132 genes between the two conditions (**Fig. 1C, detailed in**
170 **Table S1**). While the precise number of genes required for kDNA maintenance is unknown, it is
171 likely from the large number of hits identified under either condition that a considerable portion
172 of the identified genes represent false positives. For example, only a small fraction of the genes
173 from both hit lists encode proteins with experimentally determined mitochondrial localizations
174 (36), contrary to what would be expected for most kDNA maintenance factors (**Table S2**).
175 Specifically, the 'Day 5 +tet kDNA^0' vs. 'Day 0' and 'Day 5 +tet kDNA^0' vs. 'Day 5 -tet
176 kDNA^0' hit lists included only 249 (13.4%) and 85 (19.5%) genes encoding proteins with
177 mitochondrial localization. Indeed, these percentages are similar to the percentage of genes
178 encoding mitochondrial proteins (1,650, or 14.0%, according to the latest estimate (36)) among
179 all 11,764 annotated genes in the reference genome (45). In addition, of the 63 genes reported to
180 date (36) that encode kDNA-associated proteins, only 11 and 13, respectively, were included in
181 our two hit lists (**Table S2**), suggesting false negatives as well. Notably, however, the 132 genes

182 identified in both comparisons showed an enrichment for genes encoding mitochondrial proteins
183 (32 genes, or 24%), including seven previously confirmed to be associated with the kinetoplast
184 (36) (**Fig. 1C, Table S2**).

185 We therefore considered these 132 genes as our primary list of candidates. **Fig. 2** visualizes
186 this selection, including published genome-wide data on localization (36, 46), the experimentally
187 determined mitochondrial proteome of *T. brucei* (47–49), as well as currently known kDNA
188 maintenance factors (16) (see also **Table S2**). Encouragingly, when candidates were ranked
189 based on the false discovery rate (FDR) for the 'Day 5 +tet kDNA^0' vs. 'Day 5 -tet kDNA^0'
190 comparison, the top 20 included six genes encoding experimentally confirmed kDNA
191 maintenance factors (four TAC components and two enzymes involved in replication): *TAC60*
192 (50) (*Tb927.7.1400*, rank 1), *primase 2* (22) (*Tb927.1.4010*, rank 2), *TAC65* (51) (*Tb927.5.830*,
193 rank 4), *mitochondrial DNA polymerase I protein B* (29) (*Tb927.11.4690*, rank 5), *p166* (33, 52)
194 (*Tb927.11.3290*, rank 11) and *TAC102* (53) (*Tb927.7.2390*, rank 16) (**Table 1, Table S2**).

195 In addition to these six genes, four other candidates within the top 20 encode proteins with
196 experimentally confirmed mitochondrial or kinetoplast locations (**Table 1**). *Tb927.8.4240* (rank
197 7) is annotated in TriTrypDB as a hypothetical gene, universally conserved among the sequenced
198 kinetoplastids. A C-terminally tagged version of the 184 kDa protein has been localized to the
199 kinetoplast (46). Notably, *Tb927.8.4240* is a paralog of the adjacent gene *Tb927.8.4230*,
200 previously identified as encoding a putative interactor of LigK-β in a proximity labelling
201 approach (54). LigK-β and LigK-α are kDNA-associated DNA ligases (26); only LigK-α
202 expression has been successfully knocked down and shown to be essential for kDNA replication
203 (26). While *Tb*927.8.4230 localizes exclusively at the antipodal sites, analogous to *T. brucei*

204 LigK-β (26, 54), *Tb*927.8.4240 is reportedly localized in the proximity of kDNA, but not at the
205 antipodal sites themselves (54).

206 *Tb927.6.2200* (rank 8) and *Tb927.6.2190* (rank 10) are neighboring genes, and close
207 inspection of the mapped RNAi fragments revealed a fragment that included parts of both genes.
208 It is therefore possible that only one of these two genes is a genuine hit, while the other is a
209 'collateral' hit. *Tb*927.6.2200 was predicted to be a mitochondrial protein based on its
210 significantly reduced abundance in a mitochondrial fraction after ablation of ATOM40, a protein
211 critical for mitochondrial protein import (49). The human homolog of this protein, DJ-1
212 (encoded by *Park7*), is also mitochondrial and is involved in protection from oxidative stress
213 (55). *Tb*927.6.2190 is another 'conserved hypothetical' protein; its mitochondrial location was
214 experimentally confirmed in multiple studies, and its expression appears to be regulated during
215 the cell cycle (56). The final gene of interest in this subset, *Tb927.7.1910* (rank 18), encodes a
216 component of the glycine cleavage complex (57), a crucial element in mitochondrial metabolism
217 and function. This finding highlights the complex's possible involvement in kDNA maintenance,
218 potentially expanding the list of metabolic enzymes with such a dual function (58).

219 Six of the top 20 hits do not appear to encode mitochondrial proteins. *Tb927.10.13220* (rank
220 3) is annotated as a cyclophilin-type isomerase. Although some members of this family, like
221 Cyclophilin D, have important mitochondrial functions (59), this gene has been predicted to
222 encode a member of the Fam66 family of cell surface proteins (60). *Tb927.8.3860* (rank 9) has
223 been experimentally confirmed as a component of the cytosolic iron-sulfur cluster assembly
224 complex (61), which makes a putative association with kDNA maintenance unexpected.
225 *Tb927.11.16040* (rank 13) is conserved among kinetoplastids, shows some homology to
226 prefoldin-like chaperones and appears to be located in the cytoplasm. *Tb11.v5.0467* (rank 14),

227 *Tb927.10.11290* (rank 17) and *Tb11.v5.0205* (rank 20), despite their conservation among
228 kinetoplastids, possess uncertain cellular localizations (46), and lack identifiable functional
229 motifs, which adds a layer of complexity to the functional characterization of these genes. Gene
230 *Tb11.v5.0205* is identical in sequence to *Tb927.10.6130*. A tagged version of the encoded protein
231 has been localized to the cytoplasm (46). The *Tb11.v5.0467* entry in TriTrypDB includes a 5'
232 UTR of nearly 3 kb that, in part, shares 100% identity with much of the *TAC102* coding
233 sequence, suggesting that the contig that contains *Tb11.v5.0467* might be an assembly artefact
234 and that this gene is a false positive hit.

235 Finally, the top 20 candidates include a further three genes that are probably false positive
236 hits. *Tb927.916940* (rank 12) and *Tb927.9.610* (rank 15) are annotated as pseudogenes.
237 Tb927.11.4700 (rank 6) is likely a 'collateral hit': it is located next to *Tb927.11.4690* (rank 5, see
238 above) in the genome, and, similar to *Tb927.6.2200* and *Tb927.6.2190*, a close inspection of the
239 mapped RNAi fragments revealed a fragment that included parts of both genes. Thus, the
240 identification of *Tb927.11.4700* may result from its genomic proximity to a true positive hit
241 rather than involvement in kDNA maintenance.

242 **Confirmation of *Tb*927.8.4240 as a novel protein involved in kDNA maintenance**

243 Based on the above considerations, we prioritized *Tb927.8.4240* for follow-up studies. The 184
244 kDa protein product has no recognizable features or domains, except an intrinsically disordered
245 region at its C-terminus (residues 1464-1689) predicted by InterPro (62). The structural model
246 generated by AlphaFold (https://alphafold.ebi.ac.uk/entry/Q57W11) (63) has only a few domains
247 of high confidence, with limited structural similarity to the following three proteins: an
248 uncharacterized protein of *Etheostoma spectabile*, a fungal-specific transcription factor, and a
249 LisH domain-containing *Anopheles* protein. As reported previously, *Tb927.8.4240* and its

250 genomic neighbor in *T. brucei*, *Tb927.8.4230* (a gene encoding a smaller protein of 119 kDa) are
251 the closest homologs of each other in the *T. brucei* genome (E-value 9e-41 in a protein BLAST)
252 (54); they are likely paralogs that resulted from a gene duplication event. A search for potential
253 orthologs and their genomics locations in trypanosomatids using the TriTryp database
254 (www.tritrypdb.org) (64) confirms that both genes are highly conserved and usually syntenic in
255 trypanosomatids. An exception is *T. cruzi*, where a gene specific for that species has been
256 inserted between the two paralogs. Interestingly, in *T. congolense* IL3000, both genes – although
257 still syntenic with their orthologs in other trypanosomatids, appear to have degraded and are
258 annotated as pseudogenes *TcIL3000.A.H_000602900* and *TcIL3000.A.H_000603000* on
259 chromosome 8. Orthologs of *Tb927.8.4240* and *Tb927.8.4230* appear to be absent from the free-
260 living genus *Bodo* (54), the closest known relative of trypanosomatids. A syntenic *Tb927.8.4240*
261 ortholog is present in the early-branching trypanosomatid *Paratrypanosoma confusum*, but a
262 *Tb927.8.4230* ortholog is missing in this species. This suggests a scenario where the gene
263 duplication that gave rise to the two paralogs occurred after *P. confusum* had branched off;
264 however, it is also possible that the *Tb927.8.4230* ortholog was secondarily lost in that species.
265 **Fig. S2** shows sequence conservation for the orthologs from five selected trypanosomatids, *T.*
266 *brucei*, *T. vivax*, *T. cruzi*, *L. major* and *Crithidia fasciculata*. Overall, within the *Trypanosoma*
267 genus, *Tb*927.8.4240 and *Tb*927.8.4230 protein sequences are 57-59% and 43-47% identical,
268 respectively (**Fig. S2A**). Areas of relatively high conservation are concentrated in six and two
269 clusters, respectively (**Fig. S2B**; top and middle panel). Despite their common ancestry and
270 homology, the calculated isoelectric points (pI) of the two paralogs are markedly different. While
271 *Tb*927.8.4240 has a pI of 8.2, *Tb*927.8.4230 has a pI of 5.2 (note the abundance of negatively
272 charged glutamic acid and aspartic acid residues, particularly in the C-terminal region of

273 *Tb*927.8.4230; **Fig. S2B**, middle panel). In the alignment of the ten selected orthologs and
274 paralogs from the five species, areas of relatively high conservation are restricted to four regions,
275 the last three resulting from a fragmentation of the long, second region of conservation among
276 the *Tb*927.8.4230 orthologs (Fig. S2B, bottom panel; Fig. S2C).

277 To confirm the role of *Tb*927.8.4240 in kDNA maintenance, we ablated its expression in
278 bloodstream form *T. brucei* by inducible RNAi (**Fig. 3**). In two independent RNAi clones, after 3
279 days of induction, mRNA levels were reduced to ~50% and ~70%, respectively (**Fig. 3B**), which
280 resulted in a marked reduction in the population's growth rate approximately 5 days post-
281 induction (**Fig. 3A**, grey and red dashed lines). Induction of RNAi in a kDNA-independent cell
282 line (i.e. expressing γL262P) did not result in a growth phenotype (**Fig. 3A**, green lines), despite
283 a comparable reduction in mRNA levels (**Fig. 3B**), confirming a kDNA-specific growth effect.
284 After 5 days of RNAi induction, the percentage of cells in the population that had completely
285 lost their kDNA had increased substantially: from ~0.2% to >10% for 0K1N cells (i.e., cells with
286 1 nucleus but no kDNA) and from 0% to ~1% for 0K2N cells (**Fig. 3C**). In contrast, cells with
287 replicated and segregated kDNA (2K1N and 2K2N) had decreased substantially. For cells that
288 still possessed visible kDNA 5 days post-induction, a quantification of the kDNA-to-nucleus size
289 ratio at the same time point revealed an overall reduction in average kDNA size and an increased
290 variability in kDNA size (**Fig. 3D**). Even in the kDNA-independent RNAi cell line, which could
291 be observed for a longer period after induction, the percentage of 0K1N cells remained relatively
292 stable at 10% (**Fig. S2**). Depletion of *Tb*927.8.4240 in WT cells or in γL262P cells by RNAi had
293 only a very minor effect on the amount or localization of the kDNA-proximal TAC component
294 TAC102 (15, 53) (**Fig. 3E**), ruling out a role for *Tb*927.8.4240 in TAC assembly or structure.

295 Overall, these results suggested an important and specific role of *Tb*927.8.4240 in kDNA
296 maintenance. The incomplete cessation of cell growth in kDNA-dependent cells and the
297 incomplete kDNA loss in both kDNA-dependent and -independent cells could suggest some
298 intrinsic variability in parasite dependence on *Tb*927.8.4240 function, or it could be a
299 consequence of variable degrees of RNAi efficiency at the single cell level - the measured
300 reduction in mRNA levels to 50-70% represents an average across the population.

301 ***Tb*927.8.4240 shows a dynamic localization at and near the kDNA APS and at the kDNA**
302 **disk periphery**

303 To confirm the association of the *Tb*927.8.4240 protein with kDNA, we expressed a
304 hemagglutinin (HA) tagged version in procyclic form *T. brucei* and first determined the
305 approximate location by fluorescence microscopy (**Fig. 4**). Co-staining for DNA and for
306 TAC102 suggested that the *Tb*927.8.4240 protein is located at the APS.

307 To precisely localize *Tb*927.8.4240, we performed Ultrastructure Expansion Microscopy (U-
308 ExM; **Fig. 5**). Throughout the cell cycle, *Tb*927.8.4240 displayed distinct localization patterns
309 when viewed from lateral and axial perspectives (**Fig. 5A**). In G1 / early S-phase cells (1K1N),
310 we observed two punctate signals consistent with APS localization and clearly distinct from the
311 TAC when viewed laterally (**Fig. 5A$_{i}$. Fig. 5B**), while, when viewed axially, these signals either
312 appeared at a punctate distribution around the edge of the disk ('ring') or in elongated shapes at
313 opposite sites, presumably again reflecting APS localization (**Fig. 5A$_{ii,iii}$**). These two distinct
314 distributions were of similar frequency (**Fig. 5C**). In cells with dumbbell-shaped kDNA, i.e., in
315 an advanced stage of replication, *Tb*927.8.4240 signals either exhibited similar elongated shapes
316 with increased separation (**Fig. 5A$_{iv}$**) or seemed shifted to oppose each other along the replicating
317 kDNA rather than remaining antipodal (**Fig. 5A$_{v-vii}$**). The latter distribution was observed slightly

318 more frequently (**Fig. 5C**). In segregating networks, the protein localization appeared as punctate
319 rings again, with an additional localization along the 'nabelschnur' structure (65) between the
320 disks (**Fig. 5A$_{viii}$**).

321 In summary, we found that the *Tb*927.8.4240 protein shows a dynamic, cell cycle-dependent
322 localization.

323

324 **DISCUSSION**

325 Biochemical and imaging approaches have resulted in substantial progress in the identification of
326 genes involved in replication and segregation of the mitochondrial genome of trypanosomatids
327 (16, 36, 66). Using a newly developed, genome-wide genetic screening approach, we have
328 identified novel candidates for genes that are important in this process. We selected the gene
329 with systematic ID *Tb927.8.4240*, annotated as a conserved hypothetical gene
330 (www.TriTrypDB.org; (64)), for experimental follow-up.

331 Our bioinformatic analysis failed to identify any putative domains or motifs in the 184-kDa
332 *Tb*927.8.4240 protein, except an intrinsically disordered region at its C-terminus. The structure
333 predicted by AlphaFold is also not informative, as it has few domains of high confidence and
334 very limited similarity to any domains with characterized function (63). Our gene expression
335 knockdown by RNAi in bloodstream form *T. brucei* reduced the mRNA level to 50-70% and
336 produced a slow growth phenotype after 5 days, a timescale that is consistent with growth
337 phenotypes obtained in bloodstream forms for other kDNA maintenance factors (21, 67, 68). At
338 day 5 post-induction, about 10% of cells had completely lost their kDNA (0K1N, or kDNA^0),
339 and a substantial reduction in kDNA size was observed for most remaining cells. Parasites then
340 continued to grow at a slower rate, with no further increase in kDNA^0 cells. It is uncertain why
341 the percentage of kDNA^0 cells did not eventually reach 100%, even in a kDNA-independent
342 genetic background, but relatively mild growth and kDNA-loss phenotypes are not unusual after
343 RNAi-mediated ablation in bloodstream form *T. brucei*, even for essential kDNA maintenance
344 genes ((68) and references therein). The most straightforward explanations are the incomplete
345 ablation of *Tb927.8.4240* mRNA (see above) and the known variability of RNAi efficiency
346 within cell populations (69).

347 A tagged version of the *Tb*927.8.4240 protein was previously reported to localize near the
348 kDNA antipodal sites (54). Our localization studies using tagged protein and standard
349 fluorescence microscopy as well as U-ExM showed a dynamic, cell cycle-dependent location of
350 the *Tb*927.8.4240 protein. For cells at the beginning of kDNA replication, we observed two
351 alternative localizations within the population: either punctate, distributed around the rim of the
352 kDNA disk, resulting in a ring-like appearance (Fig. 6, state *a*), or signals consistent with
353 localization at antipodal sites (Fig. 6, state *b*). Viewed axially, APS localization was not dot-like,
354 as in images obtained by conventional microscopy (46), but extended along the edge of the
355 kDNA (**Fig. 6**, state *a*), similar to the recently discovered replication factor MiRF172 (21). In
356 dumbbell-shaped (or bilobed) kDNA, characteristic of cells at an advanced stage of replication,
357 the *Tb*927.8.4240 protein exhibited a similar localization patterns in ~45% of cells (**Fig. 6**, state
358 *c*), or its location was shifted along the edge of the elongated kDNA rather than remaining
359 antipodal (**Fig. 6**, state *d*). It seems reasonable to assume that state *d* develops via state *c*, rather
360 than directly from state *b*, as depicted in **Fig. 6**, although further experiments will be required to
361 confirm this. This repositioning away from the antipodal sites is reminiscent of patterns observed
362 after pulse labelling of replicating *T. brucei* minicircles with bromodeoxyuridine (BrdU), which
363 led to the development of a model of *T. brucei* kDNA replication where back-and-forth
364 oscillation of the kDNA disk facilitates a more equal distribution of daughter minicircles in the
365 replicating network (70). Later metabolic labelling experiments with the thymidine analogue 5-
366 ethynyl-2′-deoxyuridine (EdU) did not reproduce these patterns (71), and it was speculated that
367 the DNA denaturation step required for BrdU antibody detection might have resulted in imaging
368 artefacts, questioning the oscillation model (2).

369 Interestingly, in segregating networks we also observed association of some *Tb*927.8.4240
370 protein with the 'nabelschnur' (German for umbilical cord) in addition to redistribution to the
371 punctate pattern around the rim of the disk seen in state *a* (**Fig. 6**, state *e*). As the nabelschnur
372 represents maxicircle DNA that is stretched out between the segregating networks (65, 72), this
373 observation suggests that *Tb*927.8.4240 is not exclusively involved in minicircle replication.
374 Previously, only two proteins have been reported that show association with this structure, the
375 leucyl aminopeptidase *Tb*LAP1 (73) and *Tb*NAB70 (74). Similar to *Tb*927.8.4240, both proteins
376 show co-localization with the kDNA disk during replication (specifically with the kDNA
377 periphery in the case of *Tb*NAB70) and, additionally, with the nabelschnur during segregation.
378 Phenotypes for ablation are clearly distinct from what we observed for *Tb*927.8.4240, though:
379 ablation of TbLAP1 results primarily in accumulation of 2K2N cells (73), while ablation of
380 TbNAB70 prevents kDNA segregation and results in accumulation of 1K2N cells (74).

381 There is additional precedence for changes in localization of kDNA replication factors during
382 the cell cycle. For example, DNA polymerases IC and ID only accumulate at antipodal sites in
383 actively replicating networks, but are dissipated throughout the mitochondrial matrix during
384 other phases of the cell cycle (75, 76). Particularly relevant to our observation is the dynamic
385 change in expression and localization of DNA LigK-α during the cell cycle in *C. fasciculata*, this
386 enzyme being primarily observed on the faces of the kDNA disk in dividing cells, and having
387 greater localization at the KFZ face in some cells and on the opposite face in others (77). *T.*
388 *brucei* LigK-α is encoded by *Tb927.7.600*, the paralog of its neighboring gene, *LigK-β*
389 (*Tb927.7.610*). The LigK-β protein interacts with the *Tb*927.8.4240 paralog *Tb*927.8.4230 (54),
390 and both proteins are localized at the antipodal sites (26, 54). It is therefore tempting to speculate
391 that *Tb*927.8.4240 dynamically interacts with DNA LigK-α, presumably specifically in dividing

392 cells. The presence of a predicted intrinsically disordered region in Tb927.8.4240 is consistent
393 with this idea, as the conformational malleability of these domains is well suited to facilitate
394 dynamic interactions (78). This hypothesis needs to be tested in future experiments. Orthologs
395 for both DNA ligases are also neighboring genes in the *B. saltans* genome (BSAL_42315 and
396 BSAL_42320, www.TriTrypDB.org; (64)). Bodonids are free-living kinetoplastids that are a
397 sister group of the trypanosomatids, have free minicircles and lack a kDNA network structure
398 (79, 80). It has been suggested that the network structure evolved in trypanosomatids to
399 minimize minicircle loss during cell division (81). Our search of the TriTrypDB database for
400 orthologs of *Tb927.8.4230* and *Tb927.8.4240* did not find orthologs for either gene in *B. saltans*.
401 However, we identified a syntenic ortholog for *Tb927.8.4240*, but not *Tb927.8.4230*, in the early-
402 branching trypanosomatid *P. confusum*. This suggests a scenario where recruitment of
403 *Tb*927.8.4240 for kDNA replication and subsequent gene duplication and specialization of
404 paralog function evolved with the need for more sophisticated kDNA replication and segregation
405 during trypanosomatid evolution. Future studies should systematically investigate the presence
406 and absence of known kDNA replication and segregation factors in the rapidly growing number
407 of kinetoplastid genomes (82).

408 Above we described the validation and characterization of *Tb*927.8.4240 as a novel kDNA
409 maintenance factor. This, along with the identification of six known kDNA maintenance factors
410 in our top 20 list (**Table 1**) is proof-of-concept that, in principle, the genetic screen that we
411 designed for identification of kDNA maintenance factors is effective. However, the following
412 findings suggest that there is considerable room for improvement.

413 i) Of the most recent list of 63 known genes encoding kinetoplast-associated proteins, which
414 include dozens of genes where ablation has been reported to result in disruption of kDNA

415 biogenesis (16, 36), only seven are present in our list of 132 candidate genes (**Table S2**,
416 **Fig. 1**). Thus, our screen produced a considerable number of false negatives.
417 ii) The vast majority of proteins that are important for kDNA maintenance are expected to
418 have mitochondrial localization. Although there is precedence for proteins that are
419 involved in kDNA maintenance and that have an additional role outside of the
420 mitochondrion (e.g. *mitochondrial topoisomerase 2*, *Tb927.9.5590* (38, 83)), and indeed
421 we would expect some non-mitochondrial proteins with important roles in kDNA
422 maintenance (e.g. for coordination of kDNA replication and segregation with the cell
423 cycle), the number of proteins where this is the case is expected to be small. The 132
424 candidate genes include 32 genes (24%) where the protein product has been mapped to the
425 mitochondrion (36). Although this is a clear enrichment over the estimated 14% of all
426 genes that, according to a recent estimate (36), encode mitochondrial proteins, a percentage
427 of 76% non-mitochondrial proteins suggests a considerable number of false positives in
428 our list. Indeed, the list includes many genes with known functions that are not related to
429 kDNA biogenesis. Thus, our screen clearly produced a considerable number of false
430 positive hits.

431 How could the performance of the screen be improved to reduce the number of false negatives
432 and false positives? One key step in our experimental design is separation of $kDNA^+$ and $kDNA^0$
433 cells by FACS (**Fig. S1**). Although this approach separated these cell types well, it was not
434 perfect: in a control experiment with a pure population of $kDNA^+$ cells, ~0.5% of cells ended up
435 in the $kDNA^0$ gate (**Fig. S1B**). To produce enough genomic DNA for efficient amplification of
436 RNAi inserts by PCR, we cultured cells for 80 hours after sorting (see Materials & Methods).
437 Cells expressing γL262P tolerate kDNA loss well (38), but we noticed that in mixed populations

438 of kDNA$^+$ and kDNA^0 cells, the percentage of the former slowly increases. Therefore, it would
439 be beneficial to further optimize the separation of kDNA$^+$ and kDNA^0 cells by FACS and, also,
440 the PCR protocol to allow efficient amplification of RNAi inserts directly after sorting. Finally,
441 increasing the number of biological and technical replicates (we had used five biological
442 replicates for the entire procedure from RNAi induction over sorting to library preparation and
443 sequencing) would improve the identification of false hits with statistical methods.

444 Nonetheless, in addition to the characterized hit *Tb*927.8.4240, our hit list includes promising
445 candidates for prioritization in future studies. This includes three candidates in our top 20 list
446 with confirmed mitochondrial localization of the encoded proteins (*Tb927.6.2200*, *Tb927.6.2190*,
447 *Tb927.7.1910*; **Table 1**) and 22 candidates further down in the list that also encode
448 mitochondrial proteins (**Table S2**). Of particular note is *Tb927.5.520*, a gene encoding a putative
449 stomatin-like protein, as proteins with the stomatin/prohibitin/flotillin/HflK/C (SPFH) domain
450 have been reported as parts of complexes involved in maintenance of mitochondrial DNA (84).

451 In conclusion, we present an experimental strategy for a genetic screen that (i) has identified a
452 novel kDNA maintenance factor, *Tb*927.8.4240, (ii) suggests further promising candidates for
453 genes with important roles in kDNA maintenance, and (iii) points the way for second-generation
454 screens with improved performance. Our characterization of *Tb*927.8.4240 suggests that the
455 oscillation model for kDNA replication in *T. brucei* should be revisited, and that detailed and
456 systematic phylogenetic studies of the evolution of known kDNA maintenance factors in
457 kinetoplastids will be a feasible and fruitful endeavor.

458

459 # MATERIALS AND METHODS

460 ## *T. brucei* growth and whole-genome RNAi library generation

461 Bloodstream-form *T. brucei* $2T1^{T7}$ cells, resistant to blasticidin and puromycin, were cultured
462 according to the published protocol (41). Cells were maintained in HMI-11 medium (85),
463 supplemented with 10 fetal calf serum (FCS; Gibco) and 50 µg/ml penicillin/streptomycin
464 (Thermo Fisher Scientific), under a 5% CO_2 atmosphere, unless otherwise specified. A mutated
465 F_1F_O-ATPase γ subunit (γL262P) was introduced into the $2T1^{T7}$ cell line by transfection with the
466 NotI-digested pEnT6-NEO- γL262P plasmid, as described (86), and selected for resistance to
467 neomycin at a concentration of 1 µg/ml. To confirm replacement of both alleles (γL262P/γL262P
468 genotype), the relevant genomic region from selected transfectants was PCR-amplified and
469 sequenced using primers 6 and 141 (**Table S3** lists all PCR and sequencing primers for this
470 study). In contrast to the published procedure for generation of genome-wide RNAi libraries
471 (41), expression of I-SceI meganuclease did not increased recombination and transfection
472 efficiency in our cell lines. To obtain the desired library complexity, a total of 2.8×10^9 $2T1^{T7}$-
473 γL262P cells were transfected with 664 µg of the linearised pZJM RNAi library, using a total of
474 54 independent transfections (approximately 5.1×10^7 cells and 12 µg of DNA per transfection).
475 Following selection, transfected cells were grown in 300 ml of HMI-11 medium supplemented
476 with 2 µg/ml phleomycin. After five days, cells were collected by centrifugation and resuspended
477 in fresh HMI-11 medium with phleomycin, with selection continuing for an additional four days.

478 ## Fluorescence activated cell sorting

479 Fluorescence activated cell sorting (FACS) was performed using a FACSAria cell sorter (BD
480 Biosciences). *T. brucei* cells were grown under standard conditions at 37°C with 5% CO_2, using

481 HMI-11 medium with 10% FCS and antibiotics. To ensure cell vitality, the cultures were
482 maintained in the exponential growth phase, not exceeding a density of 1×10^6 cells/ml. During
483 experimental procedures, cells were centrifuged at 1200 g for 5 minutes and then resuspended in
484 Creek's Minimal Media (CMM) (87) with an additional 10% FCS, followed by a recovery period
485 of 2-3 hours at a lowered density of 5×10^5 cells/ml. Post-recovery, the cells were labeled with
486 dsFLUOR dye (Promega, E2671) for 2 minutes at a ratio of 1 µl dye per 4 ml of cell suspension.
487 Preparing for fluorescence-activated cell sorting (FACS), the cells were treated with 10 µg/ml
488 dihydroethidium (DHE), freshly made from a stock solution of 5 mg DHE in 500 µl DMSO, and
489 incubated for 20 minutes at 37°C in the dark. Subsequently, the cells were washed three times
490 with CMM containing 4% FCS (1200g for 5 minutes), which had been pre-filtered through a 50
491 µm filter to eliminate any FCS aggregates that might affect the FACS process. Lastly, the cells
492 were resuspended at a concentration of about 2×10^7 cells/ml for sorting. To reduce nonspecific
493 staining, sorting was conducted at a temperature of 10°C. Sorted cells were cultured for 80 hours
494 to produce sufficient material for PCR amplification of RNAi inserts. Sorting was carried out for
495 five independent biological replicates each, uninduced or induced for RNAi for 5 days.

496 **DNA deep sequencing**

497 To amplify RNAi target fragments from the genomic DNA, we followed a previously described
498 PCR protocol using LIB2f and LIB2r primers (41). After amplification, DNA was sent for
499 Illumina deep sequencing (BGI, Hongkong; 100PE, HiSeq 4000). Paired end sequences were
500 scanned for the presence of each primer subsequence (F=CCCCTCGAGG,
501 R=ATCAAGCTTGGCC) and trimmed using a custom script to remove extraneous bases as
502 appropriate. The resulting fasta output files for F, R and UNK (unknown) for each sample were
503 aligned to the *T. brucei* TREU927 genome (Release 42 / v5.1 from TriTrypDB.org) using

504 bowtie2 (version 2.2.7) (88) and parameters --very-sensitive -p 20 --no-unal. The resulting BAM
505 files were sorted and indexed using SAMtools (version 1.12) (89), and alignment counts to
506 predicted genes were generated from the BAM files with the appropriate bed file and BEDtools
507 (v2.23.0) (90) using the multicov -bams *.bam command. The raw gene counts output from
508 BEDtools was subsequently processed in R.

509 **RIT-seq data analysis**

510 The statistical analysis of the RIT-seq data was performed in the R environment using edgeR
511 package (91). The number of reads mapping to each CDS for each condition (5 days induced
512 sorted, 5 days non-induced sorted and day 0 non-sorted populations; 5 replicates each) were
513 normalized and log-transformed by the function calcNormFactors [trimmed mean of M-values
514 (TMM) normalization].

515 **Construction of RNAi cell lines**

516 The inducible stem-loop RNAi construct targeting gene Tb927.8.4240 was generated using the
517 pQuadra system (92). Nucleotides 1-530 of the 8.4240 gene were amplified via PCR using
518 primers 1722 and 1723 (**Table S3**). The oligonucleotides included specifically designed BstXI
519 restriction sites to facilitate directional cloning (92). Ligation with BstXI-digested pQuadra1 and
520 pQuadra3 plasmids generated pQuadra-8.4240, containing inverted repeats of the PCR product
521 separated by a spacer region, which were confirmed by sequencing the plasmid using primers
522 116, 102 and 82 (**Table S3**). The NotI-linearized construct was then introduced via nucleofection
523 (93) into *T. brucei* Lister 427 'single marker' bloodstream form cells, which express the T7 RNA
524 polymerase and tetracycline repressor protein (94). Transgenic cell lines harboring the inducible
525 RNAi cassette were selected with phleomycin. Subsequently, kDNA-independent (γL262P) and

526 kDNA-dependent control (γWT) cell lines were constructed in this RNAi background by
527 transfection with linearized pEnT6-PURO-γL262P and -γWT plasmids, respectively, as
528 described previously (86).

529 **Quantitative real-time PCR**

530 RNA from 1×10^8 cells was isolated using the RNeasy Mini Kit (Qiagen). cDNA was synthesized
531 from 1 µg of total RNA using the High-Capacity cDNA Reverse Transcription Kit (Applied
532 Biosystems). Tb927.8.4240 RT-PCR was performed using 2 µl of a 1/10 dilution of cDNA, 10 µl
533 of PowerUp SYBR Green Master Mix (Applied Biosystems), and 1 µl of 10 µM primer pair
534 1777/1778 (**Table S3**) using a Roche LightCycler. Analysis of the data was performed using the
535 2^-ΔΔCT method for relative quantification (95) with telomerase reverse transcriptase (TERT;
536 Tb927.11.10190) as the reference gene (96) (primers 1358/1359, **Table S3**).

537 **Standard fluorescence microscopy**

538 Standard fluorescence microscopy was performed as described previously (86). Briefly, cells
539 were fixed with 2% (w/v) cold formaldehyde in phosphate buffered saline (PBS), washed once
540 with PBS (1000 g, 5 min), and mounted on microscopy slides. DNA was visualized using
541 Prolong Gold antifade reagent with 4′,6-diamidino-2-phenylindole (DAPI; Life Technologies),
542 and images were captured using a Retiga 2000R Mono Cooled charged-coupled device camera
543 attached to an Axioscope 2 or Axioimager Z2 (Carl Zeiss MicroImaging, Inc.) using either Plan-
544 Apochromat 63x (1.40 NA) or Plan-Apochromat 100x (1.40 NA) phase-contrast objectives. The
545 relative amount of DAPI-stained DNA was quantified using ImageJ software (97).

546 **Ultrastructure Expansion Microscopy (U-ExM)**

547 Coverslips (12 mm, Epredia) were functionalized with poly-D-lysine (A3890401, Gibco) at
548 room temperature for 30 min, followed by three washes with deionized water. Cells were then
549 spread onto the coverslips and allowed to settle at room temperature for 10 min, fixed with 4%
550 paraformaldehyde (PFA) for 10 min and permeabilized with 0.2% Triton X-100 in PBS for 5
551 min. Cells were washed twice with PBS and samples blocked with 4% bovine serum albumin
552 (BSA) in PBS. Primary and secondary antibodies (see below for specifications) were diluted in
553 PBS containing 2% BSA and were incubated for 45 min in between PBS washes. After the last
554 wash with PBS, cells were anchored in PBS containing 0.7% formaldehyde (Sigma) and 1%
555 acrylamide (AA; Sigma) at 37°C for 2 h. Gelation was performed using a freshly prepared
556 solution composed of 19% sodium acrylate (Sigma), 10% AA, and 0.1% N,N'-
557 methylenebisacrylamide (Sigma), supplemented with 0.5% ammonium persulfate (Thermo
558 Fisher) and 0.5% tetramethylethylenediamine (Thermo Fisher). For gelation, 35 µl droplets of
559 gelation solution were placed onto parafilm within a pre-cooled humidity chamber. Coverslips
560 containing anchored cells were inverted onto droplets and incubated on ice for 5 min, followed
561 by incubation at 37°C for 30 min to allow polymerization.

562 Gels were gently detached from the coverslips by incubating in 1 ml denaturation buffer (200
563 mM SDS, 200 mM NaCl, 50 mM Tris in deionized water, pH 9) with gentle shaking at room
564 temperature for 15 min. Subsequently, gels underwent denaturation in the same buffer at 95°C
565 for 30 min. After denaturation, gels were washed three times for 5 min each with PBS, then
566 incubated for 1 h at room temperature with gentle agitation in PBS containing DAPI (5 µg/ml;
567 Sigma) for DNA staining. Following staining, gels were expanded overnight in deionized water.

568 Antibodies were used as follows:

569 • anti-HA tag antibody, rabbit, 1:1000 (Thermo Fisher)

570 • Goat anti-Rabbit IgG (H+L) Cross-Adsorbed Secondary Antibody, Alexa Fluor™ 594,
571 1:1000 (Thermo Fisher)

572 • Mouse monoclonal anti-TAC102 (53), 1:1000

573 • Goat anti-Mouse IgG (H+L) Cross-Adsorbed Secondary Antibody, Alexa Fluor™ 488
574 (Thermo Fisher)

575 • Guinea pig anti-α-tubulin, 1:500 (ABCD Antibodies)

576 • Guinea pig anti-β-tubulin, 1:500 (ABCD Antibodies)

577 • anti-guinea pig IgG Alexa Fluor 647, 1:500 (Sigma-Aldrich)

578 Expanded gels were sectioned and mounted onto poly-D-lysine-coated 25 mm glass-bottom
579 dishes (Cellvis, 35 mm dish with 20 mm microwell #1.5 cover glass). Z-stack imaging was
580 performed using a Nikon Ti2 Kinetix Widefield Microscope equipped with a 100x objective (NA
581 = 1.45). Imaging parameters included a z-step size of 0.2 µm and a pixel size of 65 nm. Images
582 were deconvolved using Huygens HRM software and analyzed in ImageJ (97).

583

584 **SUPPLEMENTAL MATERIAL**

585 Supplemental figures S1-S3

586 Tables S1-S3

587

588 **ACKNOWLEDGMENTS**

This work was supported by Senior Non-Clinical Fellowship MR/L019701/1 from the UK Medical Research Council to A.S. and an Institutional Strategic Support Fund (ISSF3) award (reference IS3-R2.28) to A.S. for a salary for M.M. and consumables. Furthermore, the work was supported by a Swiss National Science Foundation grant (number 207525) and a grant from the Uniscientia foundation to T.O. and by a Wellcome Investigator Award (217105/Z/19/Z) to D.H..

595 # REFERENCES

596 1. Stuart K, Brun R, Croft S, Fairlamb A, Gürtler RE, McKerrow J, Reed S, Tarleton R. 2008.
597 Kinetoplastids: related protozoan pathogens, different diseases. The Journal of Clinical
598 Investigation 118:1301–10.

599 2. Jensen RE, Englund PT. 2012. Network News: The Replication of Kinetoplast DNA. Annual Review
600 of Microbiology 66:473–491.

601 3. Kay C, Williams TA, Gibson W. 2020. Mitochondrial DNAs provide insight into trypanosome
602 phylogeny and molecular evolution. BMC Evolutionary Biology 20:161.

603 4. Alfonzo JD, Thiemann O, Simpson L. 1997. The mechanism of U insertion/deletion RNA editing in
604 kinetoplastid mitochondria. Nucleic acids research 25:3751–9.

605 5. Schnaufer A, Domingo GJ, Stuart K. 2002. Natural and induced dyskinetoplastic trypanosomatids:
606 how to live without mitochondrial DNA. International Journal for Parasitology 32:1071–1084.

607 6. Lukes J, Hashimi H, Zíková A. 2005. Unexplained complexity of the mitochondrial genome and
608 transcriptome in kinetoplastid flagellates. Current genetics 48:277–99.

609 7. Ogbadoyi EO, Robinson DR, Gull K. 2003. A High-Order Trans -Membrane Structural Linkage Is
610 Responsible for Mitochondrial Genome Positioning and Segregation by Flagellar Basal Bodies in
611 Trypanosomes. Molecular Biology of the Cell 14:1769–1779.

612 8. Englund PT. 2014. A passion for parasites. The Journal of biological chemistry 289:33712–29.

613 9. He P, Katan AJ, Tubiana L, Dekker C, Michieletto D. 2023. Single-Molecule Structure and Topology
614 of Kinetoplast DNA Networks. Phys Rev X 13:021010.

615 10. Schneider A. 2001. Unique aspects of mitochondrial biogenesis in trypanosomatids. International
616 Journal for Parasitology 31:1403–1415.

617 11. Aphasizheva I, Alfonzo J, Carnes J, Cestari I, Cruz-Reyes J, Göringer HU, Hajduk S, Lukeš J, Madison-
618 Antenucci S, Maslov DA, McDermott SM, Ochsenreiter T, Read LK, Salavati R, Schnaufer A,
619 Schneider A, Simpson L, Stuart K, Yurchenko V, Zhou ZH, Zíková A, Zhang L, Zimmer S, Aphasizhev
620 R. 2020. Lexis and Grammar of Mitochondrial RNA Processing in Trypanosomes. Trends in
621 Parasitology 36:337–355.

622 12. Cooper S, Wadsworth ES, Ochsenreiter T, Ivens A, Savill NJ, Schnaufer A. 2019. Assembly and
623 annotation of the mitochondrial minicircle genome of a differentiation-competent strain of
624 Trypanosoma brucei. Nucleic acids research 47:11304–11325.

625 13. Gould MK, Schnaufer A. 2014. Independence from Kinetoplast DNA Maintenance and Expression Is
626 Associated with Multidrug Resistance in Trypanosoma brucei In Vitro. Antimicrobial Agents and
627 Chemotherapy 58:2925–2928.

628 14. Roy Chowdhury A, Bakshi R, Wang J, Yildirir G, Liu B, Pappas-Brown V, Tolun G, Griffith JD, Shapiro
629 T a, Jensen RE, Englund PT. 2010. The killing of African trypanosomes by ethidium bromide. PLoS
630 Pathogens 6:e1001226.

631 15. Schneider A, Ochsenreiter T. 2018. Failure is not an option – mitochondrial genome segregation in
632 trypanosomes. Journal of Cell Science 131:jcs221820.

633 16. Amodeo S, Bregy I, Ochsenreiter T. 2022. Mitochondrial genome maintenance - the kinetoplast
634 story. FEMS Microbiol Rev fuac047.

635 17. Drew ME, Englund PT. 2001. Intramitochondrial Location and Dynamics of Crithidia fasciculata
636 Kinetoplast Minicircle Replication Intermediates. The Journal of Cell Biology 153:735–744.

637 18. Bruhn DF, Mozeleski B, Falkin L, Klingbeil MM. 2010. Mitochondrial DNA polymerase POLIB is
638 essential for minicircle DNA replication in African trypanosomes. Molecular Microbiology 75:1414–
639 25.

640 19. Milman N, Motyka SA, Englund PT, Robinson D, Shlomai J. 2007. Mitochondrial origin-binding
641 protein UMSBP mediates DNA replication and segregation in trypanosomes. Proceedings of the
642 National Academy of Sciences of the United States of America 104:19250–5.

643 20. Wang Z, Englund PT. 2001. RNA interference of a trypanosome topoisomerase II causes
644 progressive loss of mitochondrial DNA. The EMBO journal 20:4674–83.

645 21. Amodeo S, Jakob M, Ochsenreiter T. 2018. Characterization of the novel mitochondrial genome
646 replication factor MiRF172 in Trypanosoma brucei. Journal of cell science 131:pii: jcs211730.

647 22. Hines JC, Ray DS. 2011. A second mitochondrial DNA primase is essential for cell growth and
648 kinetoplast minicircle DNA replication in Trypanosoma brucei. Eukaryotic Cell 10:445–54.

649 23. Liu B, Wang J, Yaffe N, Lindsay ME, Zhao Z, Zick A, Shlomai J, Englund PT. 2009. Trypanosomes have
650 six mitochondrial DNA helicases with one controlling kinetoplast maxicircle replication. Molecular
651 Cell 35:490–501.

652 24. Liu B, Wang J, Yildirir G, Englund PT. 2009. TbPIF5 is a Trypanosoma brucei mitochondrial DNA
653 helicase involved in processing of minicircle Okazaki fragments. PLoSPathog 5:e1000589.

654 25. Saxowsky TT, Choudhary G, Klingbeil MM, Englund PT. 2003. Trypanosoma brucei Has Two Distinct
655 Mitochondrial DNA Polymerase β Enzymes. Journal of Biological Chemistry 278:49095–49101.

656 26. Downey N, Hines JC, Sinha KM, Ray DS. 2005. Mitochondrial DNA ligases of Trypanosoma brucei.
657 Eukaryot Cell 4:765–774.

658 27. Amodeo S, Bregy I, Ochsenreiter T. 2023. Mitochondrial genome maintenance-the kinetoplast
659 story. FEMS Microbiol Rev 47:fuac047.

660 28. Carpenter LR, Englund PT. 1995. Kinetoplast maxicircle DNA replication in Crithidia fasciculata and
661 Trypanosoma brucei. Molecular and Cellular Biology 15:6794–6803.

662 29. Klingbeil MM, Motyka SA, Englund PT. 2002. Multiple mitochondrial DNA polymerases in
663 Trypanosoma brucei. Mol Cell 10:175–186.

664 30. Chandler J, Vandoros AV, Mozeleski B, Klingbeil MM. 2008. Stem-loop silencing reveals that a third
665 mitochondrial DNA polymerase, POLID, is required for kinetoplast DNA replication in
666 trypanosomes. Eukaryot Cell 7:2141–2146.

667 31. Aeschlimann S, Kalichava A, Schimanski B, Berger BM, Jetishi C, Stettler P, Ochsenreiter T,
668 Schneider A. 2022. Single p197 molecules of the mitochondrial genome segregation system of
669 Trypanosoma brucei determine the distance between basal body and outer membrane.
670 Proceedings of the National Academy of Sciences 119:e2204294119.

671 32. Jetishi C, Aeschlimann S, Schimanski B, Käser S, Mullner R, Oeljeklaus S, Akiyoshi B, Warscheid B,
672 Butter F, Schneider A, Ochsenreiter T. 2025. Connecting basal body and mitochondrial DNA: TAC53
673 and the tubular organization of the tripartite attachment complex. PLoS Pathog 21:e1013521.

674 33. Schimanski B, Aeschlimann S, Stettler P, Käser S, Gomez-Fabra Gala M, Bender J, Warscheid B,
675 Vögtle F-N, Schneider A. 2022. p166 links membrane and intramitochondrial modules of the
676 trypanosomal tripartite attachment complex. PLOS Pathogens 18:e1010207.

677 34. Baudouin HCM, Pfeiffer L, Ochsenreiter T. 2020. A comparison of three approaches for the
678 discovery of novel tripartite attachment complex proteins in Trypanosoma brucei. PLOS Neglected
679 Tropical Diseases 14:e0008568.

680 35. Amodeo S, Bregy I, Hoffmann A, Fradera-Sola A, Kern M, Baudouin H, Zuber B, Butter F,
681 Ochsenreiter T. 2023. Characterization of two novel proteins involved in mitochondrial DNA
682 anchoring in Trypanosoma brucei. PLoS Pathog 19:e1011486.

683 36. Pyrih J, Hammond M, Alves A, Dean S, Sunter JD, Wheeler RJ, Gull K, Lukeš J. 2023. Comprehensive
684 sub-mitochondrial protein map of the parasitic protist Trypanosoma brucei defines critical features
685 of organellar biology. Cell Rep 42:113083.

686 37. Horn D. 2022. Genome-scale RNAi screens in African trypanosomes. Trends in parasitology
687 38:160–173.

688 38. Dean S, Gould MK, Dewar CE, Schnaufer AC. 2013. Single point mutations in ATP synthase
689 compensate for mitochondrial genome loss in trypanosomes. Proceedings of the National
690 Academy of Sciences 110:14741–14746.

691 39. Morris JC, Wang Z, Drew ME, Englund PT. 2002. Glycolysis modulates trypanosome glycoprotein
692 expression as revealed by an RNAi library. The EMBO Journal 21:4429–4438.

693 40. Alsford S, Turner DJ, Obado SO, Sanchez-Flores A, Glover L, Berriman M, Hertz-Fowler C, Horn D.
694 2011. High-throughput phenotyping using parallel sequencing of RNA interference targets in the
695 African trypanosome. Genome research 21:915–24.

696 41. Glover L, Alsford S, Baker N, Turner DJ, Sanchez-Flores A, Hutchinson S, Hertz-Fowler C, Berriman
697 M, Horn D. 2015. Genome-scale RNAi screens for high-throughput phenotyping in bloodstream-
698 form African trypanosomes. Nature protocols 10:106–33.

699 42. Wang Z, Drew ME, Morris JC, Englund PT. 2002. Asymmetrical division of the kinetoplast DNA
700 network of the trypanosome. The EMBO journal 21:4998–5005.

701 43. Ashley N, Harris D, Poulton J. 2005. Detection of mitochondrial DNA depletion in living human cells
702 using PicoGreen staining. Experimental cell research 303:432–46.

703 44. Amodeo S, Kalichava A, Fradera-Sola A, Bertiaux-Lequoy E, Guichard P, Butter F, Ochsenreiter T.
704 2021. Characterization of the novel mitochondrial genome segregation factor TAP110 in
705 Trypanosoma brucei. Journal of cell science 134:jcs.254300.

706 45. Alvarez-Jarreta J, Amos B, Aurrecoechea C, Bah S, Barba M, Barreto A, Basenko EY, Belnap R,
707 Blevins A, Böhme U, Brestelli J, Brown S, Callan D, Campbell LI, Christophides GK, Crouch K,
708 Davison HR, DeBarry JD, Demko R, Doherty R, Duan Y, Dundore W, Dyer S, Falke D, Fischer S, Gajria
709 B, Galdi D, Giraldo-Calderón GI, Harb OS, Harper E, Helb D, Howington C, Hu S, Humphrey J, Iodice
710 J, Jones A, Judkins J, Kelly SA, Kissinger JC, Kittur N, Kwon DK, Lamoureux K, Li W, Lodha D,
711 MacCallum RM, Maslen G, McDowell MA, Myers J, Nural MV, Roos DS, Rund SSC,
712 Shanmugasundram A, Sitnik V, Spruill D, Starns D, Tomko SS, Wang H, Warrenfeltz S, Wieck R,
713 Wilkinson PA, Zheng J. 2024. VEuPathDB: the eukaryotic pathogen, vector and host bioinformatics
714 resource center in 2023. Nucleic Acids Res 52:D808–D816.

715 46. Billington K, Halliday C, Madden R, Dyer P, Barker AR, Moreira-Leite FF, Carrington M, Vaughan S,
716 Hertz-Fowler C, Dean S, Sunter JD, Wheeler RJ, Gull K. 2023. Genome-wide subcellular protein map
717 for the flagellate parasite Trypanosoma brucei. Nat Microbiol 8:533–547.

718 47. Zíková A, Verner Z, Nenarokova A, Michels PAM, Lukeš J. 2017. A paradigm shift: The
719 mitoproteomes of procyclic and bloodstream Trypanosoma brucei are comparably complex. PLoS
720 pathogens 13:e1006679.

721 48. Panigrahi AK, Ogata Y, Zíková A, Anupama A, Dalley RA, Acestor N, Myler PJ, Stuart KD. 2009. A
722 comprehensive analysis of Trypanosoma brucei mitochondrial proteome. Proteomics 9:434–50.

723 49. Peikert CD, Mani J, Morgenstern M, Käser S, Knapp B, Wenger C, Harsman A, Oeljeklaus S,
724 Schneider A, Warscheid B. 2017. Charting organellar importomes by quantitative mass
725 spectrometry. Nature Communications 8:15272.

726 50. Käser S, Willemin M, Schnarwiler F, Schimanski B, Poveda-Huertes D, Oeljeklaus S, Haenni B, Zuber
727 B, Warscheid B, Meisinger C, Schneider A. 2017. Biogenesis of the mitochondrial DNA inheritance
728 machinery in the mitochondrial outer membrane of Trypanosoma brucei. PLOS Pathogens
729 13:e1006808.

730 51. Käser S, Oeljeklaus S, Týč J, Vaughan S, Warscheid B, Schneider A. 2016. Outer membrane protein
731 functions as integrator of protein import and DNA inheritance in mitochondria. Proceedings of the
732 National Academy of Sciences of the United States of America 113:E4467-75.

733 52. Zhao Z, Lindsay ME, Roy Chowdhury A, Robinson DR, Englund PT. 2008. p166, a link between the
734 trypanosome mitochondrial DNA and flagellum, mediates genome segregation. The EMBO Journal
735 27:143–54.

736 53. Trikin R, Doiron N, Hoffmann A, Haenni B, Jakob M, Schnaufer A, Schimanski B, Zuber B,
737 Ochsenreiter T. 2016. TAC102 Is a Novel Component of the Mitochondrial Genome Segregation
738 Machinery in Trypanosomes. PLOS Pathogens 12:e1005586.

739 54. Pyrih J, Rašková V, Škodová-Sveráková I, Pánek T, Lukeš J. 2020. ZapE/Afg1 interacts with Oxa1 and
740 its depletion causes a multifaceted phenotype. PLOS ONE 15:e0234918.

741 55. Nam Y, Na J, Ma S-X, Park H, Park H, Lee E, Kim H, Jang S-M, Ko HS, Kim S. 2024. DJ-1 protects cell
742 death from a mitochondrial oxidative stress due to GBA1 deficiency. Genes Genomics
743 https://doi.org/10.1007/s13258-024-01506-w.

744 56. Benz C, Urbaniak MD. 2019. Organising the cell cycle in the absence of transcriptional control:
745 Dynamic phosphorylation co-ordinates the Trypanosoma brucei cell cycle post-transcriptionally.
746 PLoS Pathog 15:e1008129.

747 57. Müller M, Papadopoulou B. 2010. Stage-specific expression of the glycine cleavage complex
748 subunits in Leishmania infantum. Mol Biochem Parasitol 170:17–27.

749 58. Sykes SE, Hajduk SL. 2013. Dual functions of α-ketoglutarate dehydrogenase E2 in the Krebs cycle
750 and mitochondrial DNA inheritance in Trypanosoma brucei. Eukaryotic Cell 12:78–90.

751 59. Gauba E, Chen H, Guo L, Du H. 2019. Cyclophilin D deficiency attenuates mitochondrial F1Fo ATP
752 synthase dysfunction via OSCP in Alzheimer's disease. Neurobiol Dis 121:138–147.

753 60. Jackson AP, Allison HC, Barry JD, Field MC, Hertz-Fowler C, Berriman M. 2013. A cell-surface
754 phylome for African trypanosomes. PLoS Negl Trop Dis 7:e2121.

755 61. Tonini ML, Peña-Diaz P, Haindrich AC, Basu S, Kriegová E, Pierik AJ, Lill R, MacNeill SA, Smith TK,
756 Lukeš J. 2018. Branched late-steps of the cytosolic iron-sulphur cluster assembly machinery of
757 Trypanosoma brucei. PLoS Pathog 14:e1007326.

758 62. Blum M, Andreeva A, Florentino LC, Chuguransky SR, Grego T, Hobbs E, Pinto BL, Orr A, Paysan-
759 Lafosse T, Ponamareva I, Salazar GA, Bordin N, Bork P, Bridge A, Colwell L, Gough J, Haft DH,

760 Letunic I, Llinares-López F, Marchler-Bauer A, Meng-Papaxanthos L, Mi H, Natale DA, Orengo CA,
761 Pandurangan AP, Piovesan D, Rivoire C, Sigrist CJA, Thanki N, Thibaud-Nissen F, Thomas PD,
762 Tosatto SCE, Wu CH, Bateman A. 2025. InterPro: the protein sequence classification resource in
763 2025. Nucleic Acids Res 53:D444–D456.

764 63. Jumper J, Evans R, Pritzel A, Green T, Figurnov M, Ronneberger O, Tunyasuvunakool K, Bates R,
765 Žídek A, Potapenko A, Bridgland A, Meyer C, Kohl SAA, Ballard AJ, Cowie A, Romera-Paredes B,
766 Nikolov S, Jain R, Adler J, Back T, Petersen S, Reiman D, Clancy E, Zielinski M, Steinegger M,
767 Pacholska M, Berghammer T, Bodenstein S, Silver D, Vinyals O, Senior AW, Kavukcuoglu K, Kohli P,
768 Hassabis D. 2021. Highly accurate protein structure prediction with AlphaFold. Nature 596:583–
769 589.

770 64. Shanmugasundram A, Starns D, Böhme U, Amos B, Wilkinson PA, Harb OS, Warrenfeltz S, Kissinger
771 JC, McDowell MA, Roos DS, Crouch K, Jones AR. 2023. TriTrypDB: An integrated functional
772 genomics resource for kinetoplastida. PLoS Negl Trop Dis 17:e0011058.

773 65. Gluenz E, Shaw MK, Gull K. 2007. Structural asymmetry and discrete nucleic acid subdomains in
774 the Trypanosoma brucei kinetoplast. Molecular microbiology 64:1529–39.

775 66. Cadena LR, Svobodová M, Benz C, Rašková V, Chmelová Ľ, Škodová-Sveráková I, Yurchenko V,
776 Lukeš J, Hammond M, Durante IM. 2024. Characterization of novel and essential kinetoplast-
777 associated proteins in *Trypanosoma brucei*. Cell Biology
778 https://doi.org/10.1101/2024.04.22.590512.

779 67. Timms MW, van Deursen FJ, Hendriks EF, Matthews KR. 2002. Mitochondrial development during
780 life cycle differentiation of African trypanosomes: evidence for a kinetoplast-dependent
781 differentiation control point. Molecular Biology of the Cell 13:3747–59.

782 68. Bruhn DF, Sammartino MP, Klingbeil MM. 2011. Three mitochondrial DNA polymerases are
783 essential for kinetoplast DNA replication and survival of bloodstream form Trypanosoma brucei.
784 Eukaryotic Cell 10:734–43.

785 69. Drozdz M, Quijada L, Clayton CE. 2002. RNA interference in trypanosomes transfected with sense
786 and antisense plasmids. Mol Biochem Parasitol 121:149–152.

787 70. Liu Y, Englund PT. 2007. The rotational dynamics of kinetoplast DNA replication. Mol Microbiol
788 64:676–690.

789 71. Wang J, Englund PT, Jensen RE. 2012. TbPIF8, a Trypanosoma brucei protein related to the yeast
790 Pif1 helicase, is essential for cell viability and mitochondrial genome maintenance. Mol Microbiol
791 83:471–485.

792 72. Gluenz E, Povelones ML, Englund PT, Gull K. 2011. The kinetoplast duplication cycle in
793 Trypanosoma brucei is orchestrated by cytoskeleton-mediated cell morphogenesis. Molecular and
794 cellular biology 31:1012–21.

795 73. Peña-Diaz P, Vancová M, Resl C, Field MC, Lukeš J. 2017. A leucine aminopeptidase is involved in
796 kinetoplast DNA segregation in Trypanosoma brucei. PLoS pathogens 13:e1006310.

797 74. Cadena LR, Hammond M, Tesařová M, Chmelová Ľ, Svobodová M, Durante IM, Yurchenko V, Lukeš
798 J. 2024. A novel nabelschnur protein regulates segregation of the kinetoplast DNA in Trypanosoma
799 brucei. Curr Biol 34:4803–4812.

800 75. Concepción-Acevedo J, Luo J, Klingbeil MM. 2012. Dynamic Localization of Trypanosoma brucei
801 Mitochondrial DNA Polymerase ID. Eukaryotic Cell 11:844–855.

802 76. Concepción-Acevedo J, Miller JC, Boucher MJ, Klingbeil MM. 2018. Cell cycle localization dynamics
803 of mitochondrial DNA polymerase IC in African trypanosomes. Molecular Biology of the Cell
804 29:2540–2552.

805 77. Sinha KM, Hines JC, Ray DS. 2006. Cell cycle-dependent localization and properties of a second
806 mitochondrial DNA ligase in Crithidia fasciculata. Eukaryot Cell 5:54–61.

807 78. Holehouse AS, Kragelund BB. 2024. The molecular basis for cellular function of intrinsically
808 disordered protein regions. Nat Rev Mol Cell Biol 25:187–211.

809 79. Lukes J, Guilbride DL, Votýpka J, Zíková A, Benne R, Englund PT. 2002. Kinetoplast DNA network:
810 evolution of an improbable structure. Eukaryotic cell 1:495–502.

811 80. Blom D, De Haan A, Van den Burg J, van den Berg M, Sloof P, Jirku M, Lukes J, Benne R. 2000.
812 Mitochondrial minicircles in the free-living bodonid Bodo saltans contain two gRNA gene cassettes
813 and are not found in large networks. RNA 6:121–135.

814 81. Borst P. 1991. Why kinetoplast DNA networks? Trends in genetics : TIG 7:139–41.

815 82. Kostygov AY, Albanaz ATS, Butenko A, Gerasimov ES, Lukeš J, Yurchenko V. 2023. Phylogenetic
816 framework to explore trait evolution in Trypanosomatidae. Trends Parasitol 40:96–99.

817 83. Gaziová I, Lukes J. 2003. Mitochondrial and nuclear localization of topoisomerase II in the flagellate
818 Bodo saltans (Kinetoplastida), a species with non-catenated kinetoplast DNA. J Biol Chem
819 278:10900–10907.

820 84. Merkwirth C, Langer T. 2009. Prohibitin function within mitochondria: Essential roles for cell
821 proliferation and cristae morphogenesis. Biochimica et Biophysica Acta (BBA) - Molecular Cell
822 Research 1793:27–32.

823 85. Hirumi H, Hirumi K. 1989. Continuous cultivation of Trypanosoma brucei blood stream forms in a
824 medium containing a low concentration of serum protein without feeder cell layers. The Journal of
825 parasitology 75:985–9.

826 86. Dewar CE, MacGregor P, Cooper S, Gould MK, Matthews KR, Savill NJ, Schnaufer A. 2018.
827 Mitochondrial DNA is critical for longevity and metabolism of transmission stage Trypanosoma
828 brucei. PLoS pathogens 14:e1007195.

829 87. Creek DJ, Nijagal B, Kim D-H, Rojas F, Matthews KR, Barrett MP. 2013. Metabolomics guides
830 rational development of a simplified cell culture medium for drug screening against Trypanosoma
831 brucei. Antimicrobial Agents and Chemotherapy 57:2768–79.

832 88. Langmead B, Salzberg SL. 2012. Fast gapped-read alignment with Bowtie 2. Nature Methods
833 9:357–359.

834 89. Li H, Handsaker B, Wysoker A, Fennell T, Ruan J, Homer N, Marth G, Abecasis G, Durbin R. 2009.
835 The Sequence Alignment/Map format and SAMtools. Bioinformatics 25:2078–2079.

836 90. Quinlan AR. 2014. BEDTools: The Swiss-Army Tool for Genome Feature Analysis. Curr Protoc
837 Bioinformatics 47:11.12.1-34.

838 91. Robinson MD, McCarthy DJ, Smyth GK. 2010. edgeR: a Bioconductor package for differential
839 expression analysis of digital gene expression data. Bioinformatics 26:139–140.

840 92. Inoue M, Nakamura Y, Yasuda K, Yasaka N, Hara T, Schnaufer A, Stuart K, Fukuma T. 2005. The 14-
841 3-3 Proteins of Trypanosoma brucei Function in Motility, Cytokinesis, and Cell Cycle. Journal of
842 Biological Chemistry 280:14085–14096.

843 93. Burkard G, Fragoso CM, Roditi I. 2007. Highly efficient stable transformation of bloodstream forms
844 of Trypanosoma brucei. Molecular and Biochemical Parasitology 153:220–223.

845 94. Wirtz E, Leal S, Ochatt C, Cross GeorgeAM. 1999. A tightly regulated inducible expression system
846 for conditional gene knock-outs and dominant-negative genetics in Trypanosoma brucei.
847 Molecular and Biochemical Parasitology 99:89–101.

848 95. Livak KJ, Schmittgen TD. 2001. Analysis of relative gene expression data using real-time
849 quantitative PCR and the 2(-Delta Delta C(T)) Method. Methods 25:402–408.

850 96. Brenndörfer M, Boshart M. 2010. Selection of reference genes for mRNA quantification in
851 Trypanosoma brucei. Molecular and biochemical parasitology 172:52–5.

852 97. Arena ET, Rueden CT, Hiner MC, Wang S, Yuan M, Eliceiri KW. 2017. Quantitating the cell: turning
853 images into numbers with ImageJ. Wiley Interdisciplinary Reviews: Developmental Biology 6:e260.

854 98. Edgar RC. 2004. MUSCLE: multiple sequence alignment with high accuracy and high throughput.
855 Nucleic Acids Res 32:1792–1797.

856 99. Waterhouse AM, Procter JB, Martin DMA, Clamp M, Barton GJ. 2009. Jalview Version 2--a multiple
857 sequence alignment editor and analysis workbench. Bioinformatics 25:1189–1191.

858 100. Livingstone CD, Barton GJ. 1993. Protein sequence alignments: a strategy for the hierarchical
859 analysis of residue conservation. Comput Appl Biosci 9:745–756.

860

861

862

863 # Figures

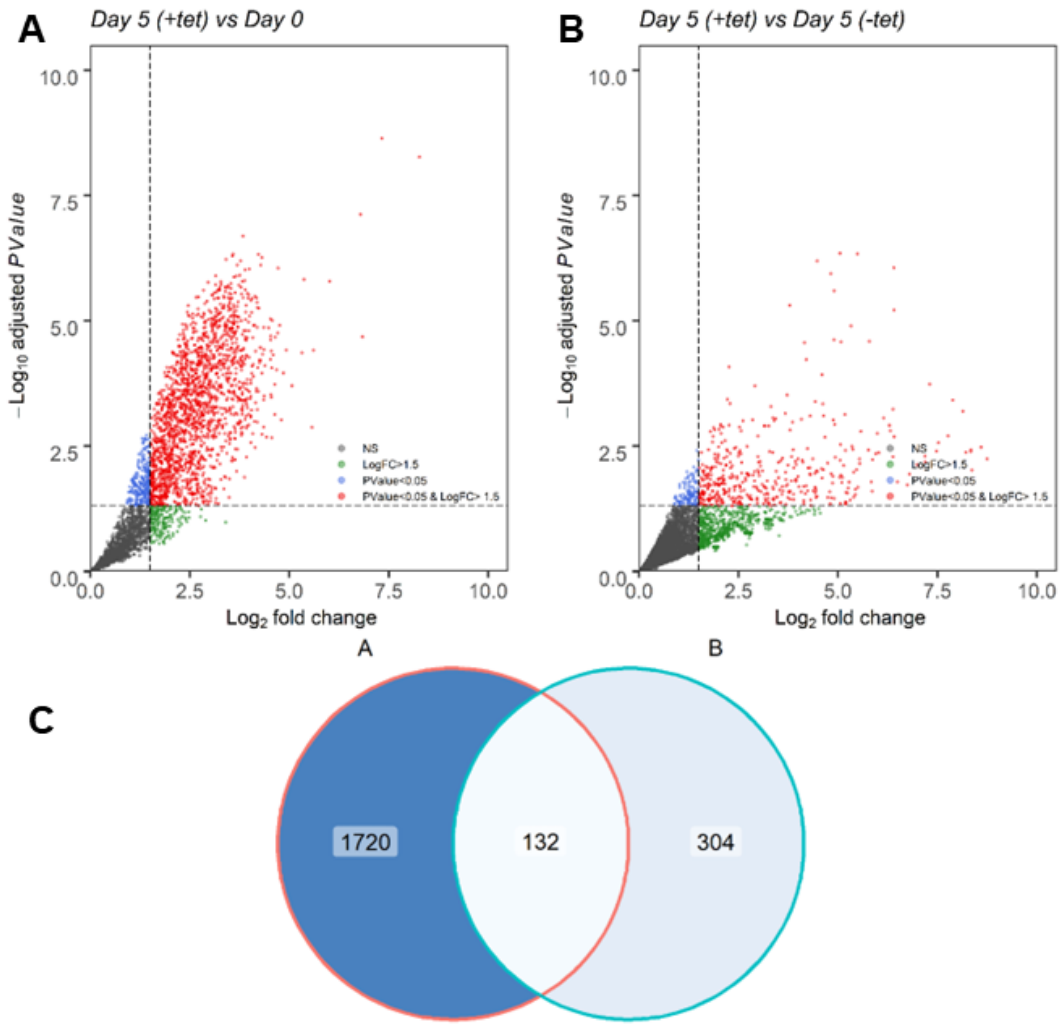

864

865 **Fig 1** Identification of putative kDNA maintenance factors by genome wide RNAi screening. (**A, B**)
866 Volcano plots showing the enrichment of genes in 'Day 5 +tet kDNA^{0}' compared to 'Day 0' (A), and 'Day 5
867 -tet kDNA^{0}' (**B**). Significant enrichment is indicated for genes with a $\log_2$ fold change ($\log_2$FC) greater than
868 1.5 and an adjusted p-value of less than 0.05, shown in red. Each dot represents a gene; green dots
869 represent non-significant (NS) genes with a $\log_2$FC less than 1.5 and/or an adjusted p-value equal to or
870 greater than 0.05. The vertical dashed line represents the $\log_2$FC threshold of 1.5, and the horizontal
871 dashed line indicates the p-value threshold of 0.05. Five biological replicates were used for all samples (n
872 = 5). (**C**) Venn diagram representing the intersection of genes identified in both comparisons.

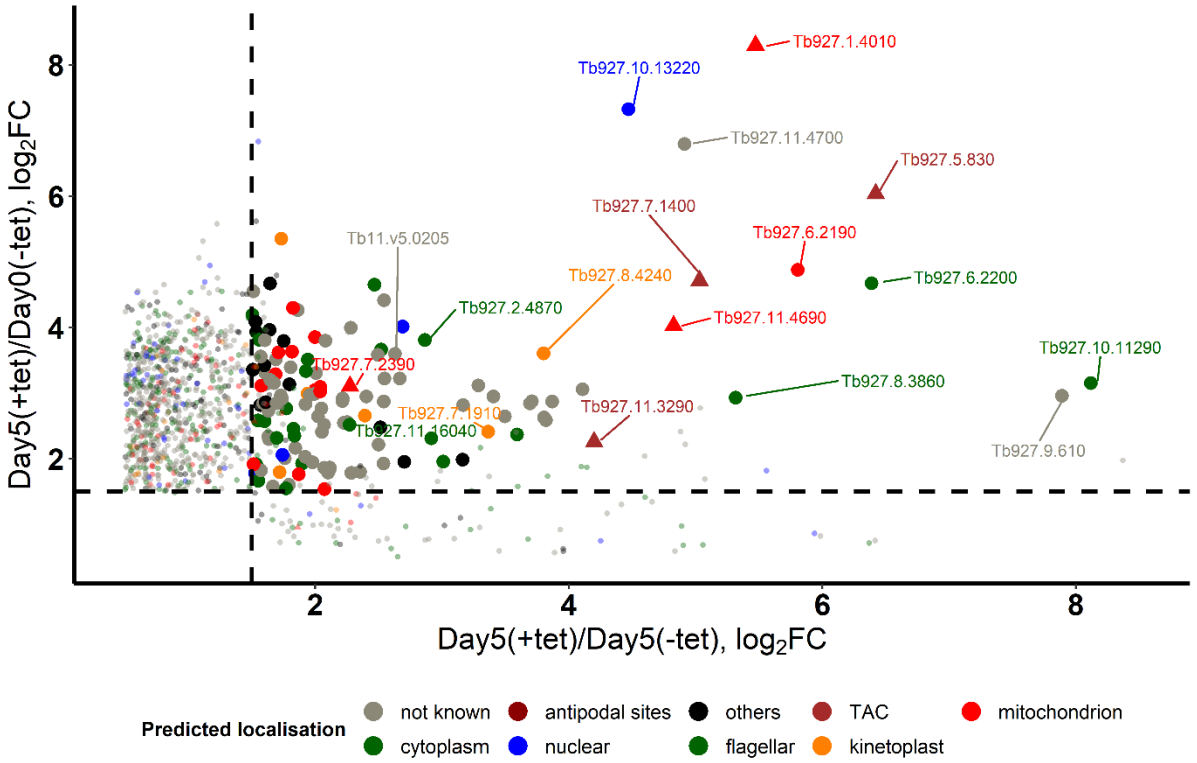

Fig 2 Visualization of primary set of 132 candidate genes implicated in kDNA maintenance, as identified through RNAi library screening. The visualized data include metadata on protein localization from TrypTag.org (36, 46), integration with published mitoproteome analyses (47–49), and previously identified kDNA maintenance factors (triangles; ref (16) and references therein). Statistically significant changes (adjusted *p*-value < 0.05) are indicated by larger circles. For clarity and reference, TriTrypDB gene identifiers are indicated for the top 20 ranked candidates based on the false discovery rate (FDR) in the y-axis comparison, detailed in Table 1 and Table S1.

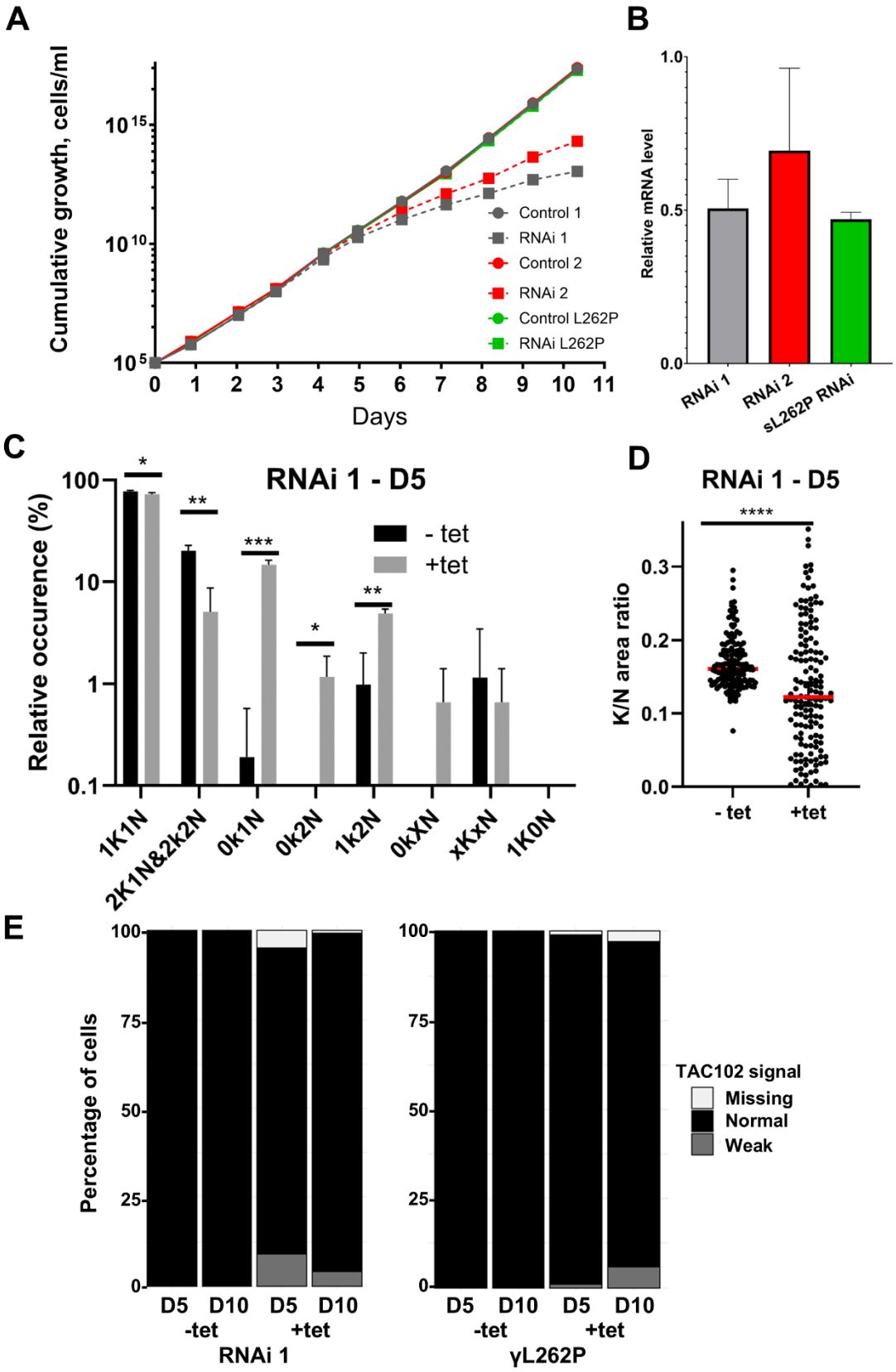
A
Cumulative growth, cells/ml
Days
Control 1
RNAi 1
Control 2
RNAi 2
Control L262P
RNAi L262P
B
Relative mRNA level
RNAi 1
RNAi 2
sL262P RNAi
C
RNAi 1 - D5
Relative occurence (%)
- tet
+tet
1K1N
2K1N&2k2N
0k1N
0k2N
1k2N
0kXN
xKxN
1K0N
D
RNAi 1 - D5
K/N area ratio
- tet
+tet
E
Percentage of cells
D5
D10
-tet
+tet
RNAi 1
γL262P
TAC102 signal
Missing
Normal
Weak

882

883 **Fig 3** Phenotypic analysis of *Tb*927.8.4240 ablation in bloodstream form *T. brucei*. (**A**) Growth phenotype
884 upon *Tb*927.8.4240 RNAi knockdown in WT cells (two independent RNAi clones (grey and red) is
885 rescued in kDNA-independent cells (introduction of γL262P mutation; green). (**B**) Levels of mRNA
886 measured by quantitative RT-PCR, at day 3 post induction (n = 3). (**C**) Quantification of relative
887 occurrence of kDNA (K) and nuclei (N) in DAPI stained cells from induced (+tet) and non-induced (-tet)
888 RNAi cell line 1 populations at day 5 post induction (n>100 cells for each triplicate; unpaired *t*-test
889 P<0.05*, <0.01**, <0.001***). (**D**) The relative amount of kDNA to nucleus area in 1K1N RNAi cell line 1 at
890 5 days post-induction (Mann-Whitney test; P<0.0001****). (**E**) *Tb*927.8.4240 RNAi knockdown in WT cells
891 or γL262P cells has only a minor effect on TAC102, as assessed with a TAC-specific antibody and
892 epifluorescence microscopy (see Fig 4A; n>100 cells for each sample; paired *t*-test P<0.05).

893

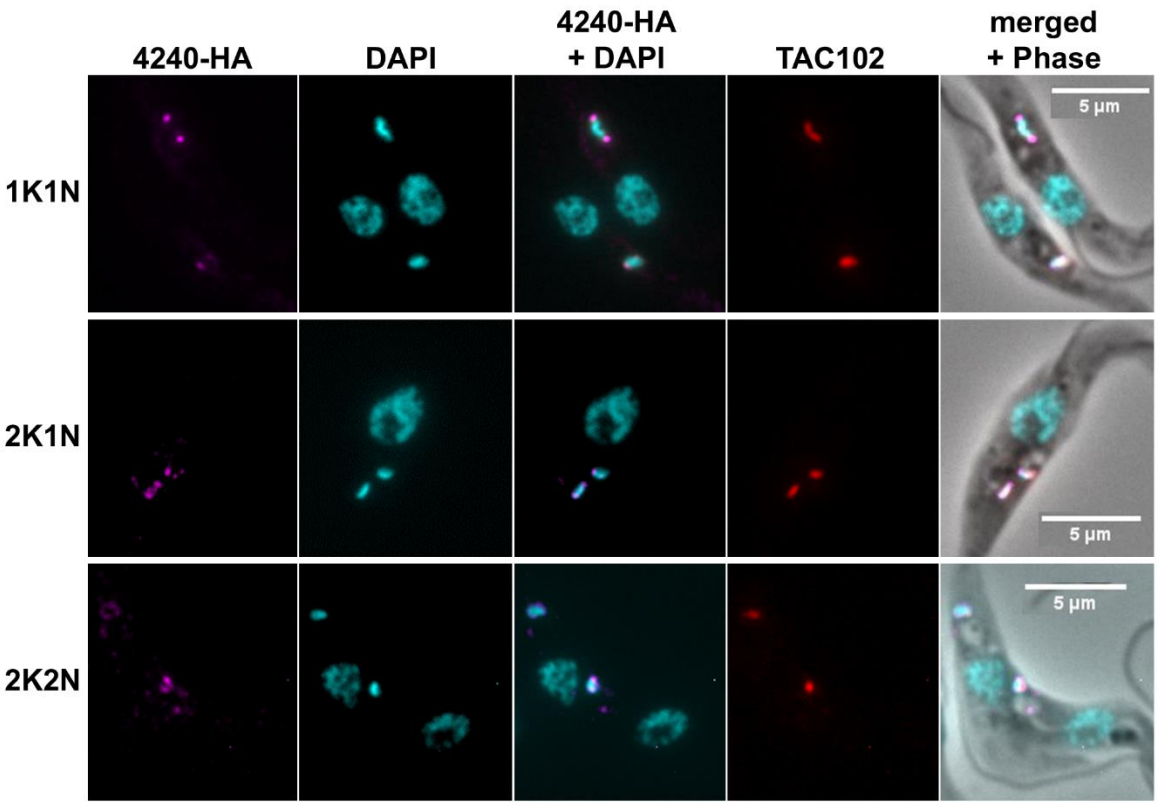

894

895

896 **Fig 4** *Tb*927.8.4240 localization in procyclic *T. brucei* throughout the cell cycle assessed using standard

897 epifluorescence microscopy. From left to right: *Tb*927.8.4240-HA tagged signal (magenta, anti-HA);

898 nuclear and kDNA (cyan, DAPI); merge of anti-HA and DAPI; TAC102 (red, anti-TAC102); merge with

899 phase contrast image. Scale bar 5 µm.

900

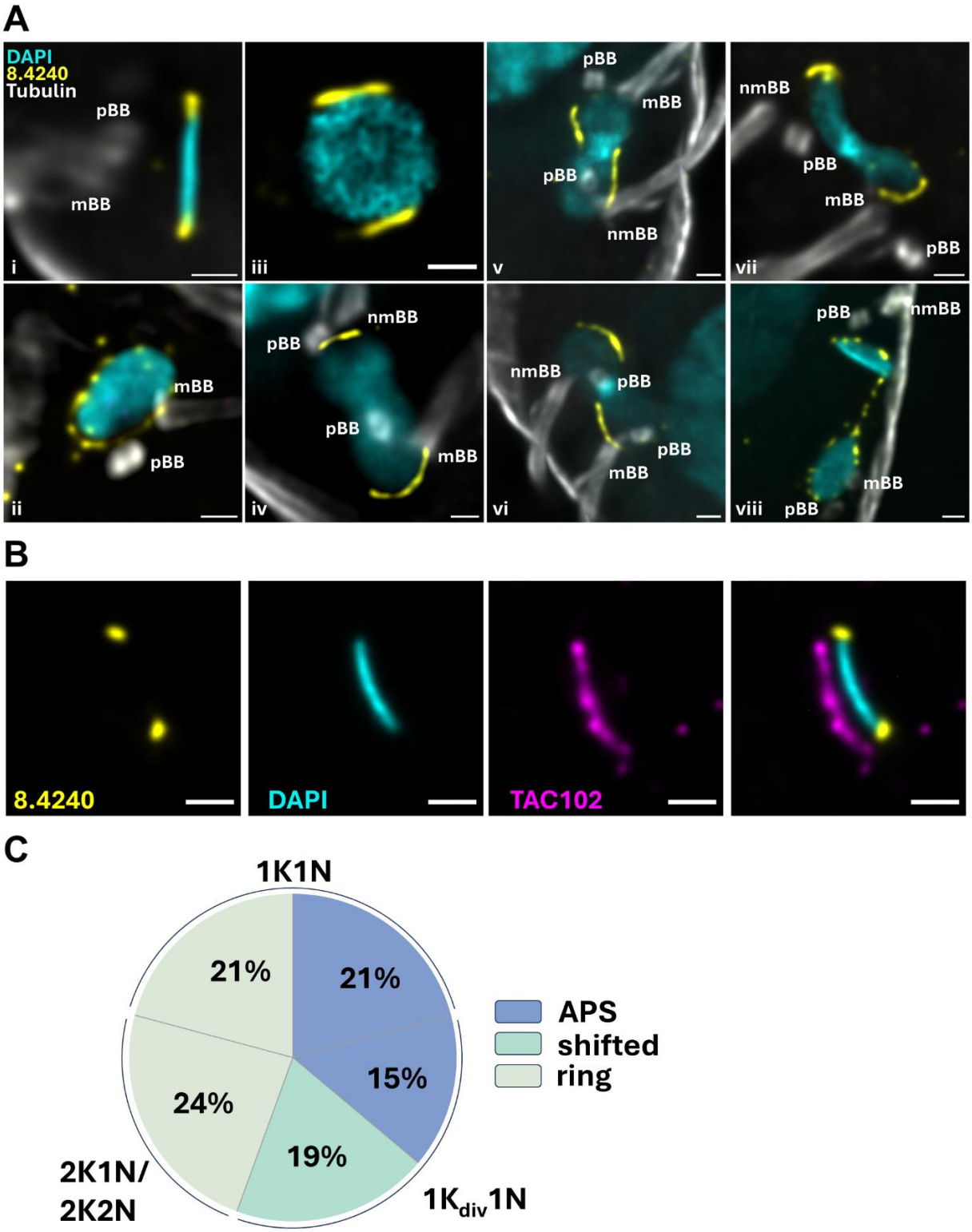
A
DAPI
8.4240
Tubulin
pBB
mBB
i
ii
iii
iv
v
vi
vii
viii
nmBB
B
8.4240
DAPI
TAC102
C
1K1N
21%
21%
15%
19%
24%
APS
shifted
ring
2K1N/
2K2N
1K$_{div}$1N

901

902

903

904 **Fig 5** *Tb*927.8.4240 localization in procyclic *T. brucei* throughout the cell cycle, determined with
905 Ultrastructure Expansion Microscopy (U-ExM). (**A**) *Tb*927.8.4240 localization pre replication (images i-iii),
906 in replicating networks (images iv-vii), and in segregating networks (image viii), from both lateral (image i)
907 and axial views (images ii-viii). *Tb*927.8.4240 is shown in yellow, kDNA in cyan, tubulin in grey; pBB, pro-
908 basal body; mBB, mature basal body, nmBB, new mature basal body. Scale bar: 1 μm. (**B**) U-ExM image
909 of *Tb*927.8.4240 (yellow) co-stained with TAC102 (magenta); kDNA is shown in cyan. Scale bar: 1 μm.
910 (**C**) Quantitation of Tb927.8.4240 localization during the cell cycle as determined by U-ExM. Configuration
911 $1K_{div}1N$ represents cells with replicating kDNA, as in images iv-vii in panel A. A total of 144 cells were
912 analyzed.

913

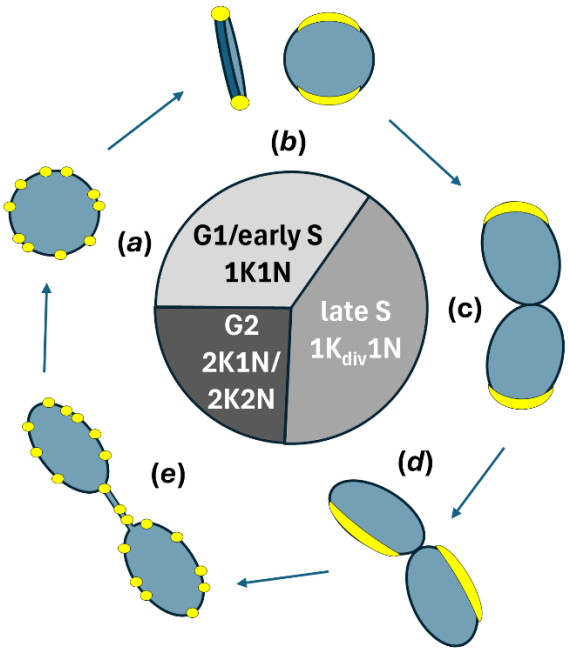

914

915

916 **Fig 6** Model for dynamic localization of *Tb*927.8.4240 during kDNA replication. The model is based on the
917 U-ExM studies shown in **Fig. 5**. Blue, kDNA; yellow, *Tb*927.8.4240 protein. Note that the respective size
918 of the cell cycle stages in the diagram is drawn simply for convenience and not proportional to their actual
919 duration. The three distinct states of localization are ring-like (a, e), antipodal (b, c) and shifted (d), in
920 accordance with **Fig. 5**.

921

922 # Tables

Rank	TriTrypDB ID	TriTrypDB Annotation	kDNA loss confirmed after knockdown	kDNA association confirmed	mitochondrial localisation confirmed	Reference(s) (PMID)
1	*Tb927.7.1400*	Tripartite Attachment Complex Protein 60	yes	yes	yes	29287109
2	*Tb927.1.4010*	primase 2	yes	yes	yes	21257796
3	*Tb927.10.13220*	cyclophilin type peptidyl-prolyl cis-trans isomerase, putative				23556014
4	*Tb927.5.830*	Tripartite attachment complex protein 65	yes	yes	yes	27436903
5	*Tb927.11.4690*	mitochondrial DNA polymerase I protein B	yes	yes	yes	12150917
6	*Tb927.11.4700*	prostaglandin f synthase				
7	*Tb927.8.4240*	hypothetical protein, conserved		yes	yes	36804636, 32579605
8	*Tb927.6.2200*	DJ-1 family protein, putative			yes	37669165
9	*Tb927.8.3860*	cytosolic iron-sulfur protein assembly 1				30346997
10	*Tb927.6.2190*	hypothetical protein, conserved			yes	37669165, 28485388
11	*Tb927.11.3290*	Tripartite attachment complex protein 166 (p166)	yes	yes	yes	18059470, 35709300
12	*Tb927.9.16940*	variant surface glycoprotein (VSG, pseudogene), putative				
13	*Tb927.11.16040*	prefoldin subunit, putative				
14	*Tb11.v5.0467*	hypothetical protein, conserved				
15	*Tb927.9.610*	hypothetical protein (pseudogene)				
16	*Tb927.7.2390*	Tripartite attachment complex protein 102	yes	yes	yes	27168148
17	*Tb927.10.11290*	hypothetical protein, conserved				
18	*Tb927.7.1910*	pyridoxal phosphate containing glycine decarboxylase, putative			yes	37669165
19	*Tb927.2.4870*	kinetoplastid-specific dual specificity phosphatase, putative				
20	*Tb927.6.1290*	hypothetical protein, conserved				

923

924 **TABLE 1** Top 20 candidates from the list of 132 primary candidates, ranked according to lowest false

925 discovery rate (FDR) in the ‘Day 5 +tet kDNA^0’ vs. ‘Day 5 -tet kDNA^0’ comparison (Table S1).

926

Supplemental Figures

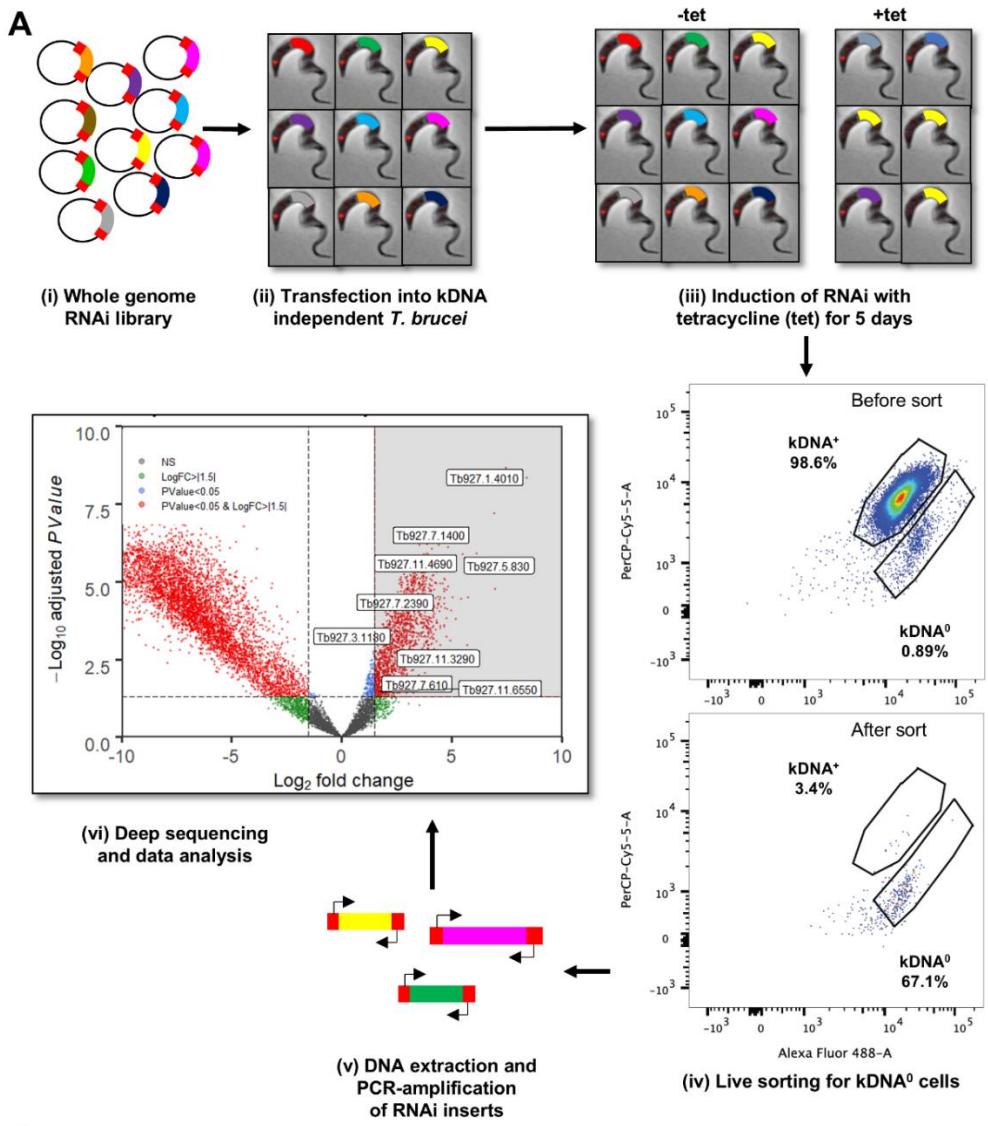

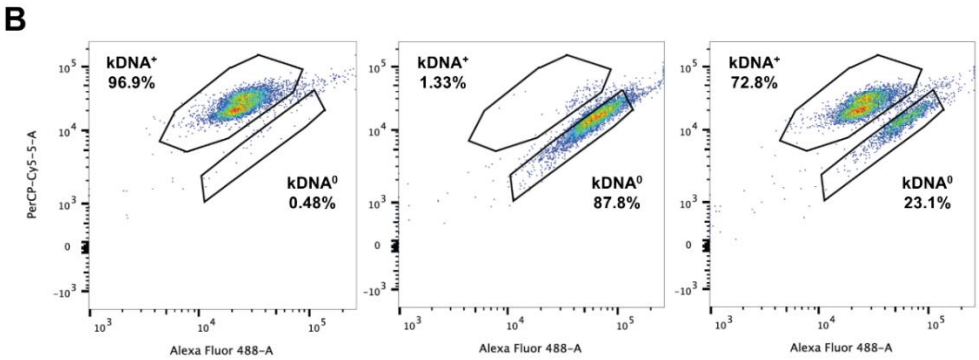

929 **Fig S1** Screening approach. (**A**) Overview of the kDNA RIT-seq experimental design to find
930 genes that are important for kDNA maintenance. (i, ii) A whole genome RNAi library (Alsford
931 et al., Genome Research 2011) was transfected into kDNA-independent *T. brucei*. (iii) Upon
932 RNAi library induction (+tet), fragments corresponding to genes essential for kDNA
933 maintenance are expected to result in the loss of kDNA from the cell. Note that induction of
934 some RNAi fragments will result in a growth defect and depletion of the cells from the
935 population, but in the kDNA-independent background this should not be the case for genes of
936 interest. (iv) To identify these genes, 5 days after induction, live cells are sorted by FACS after
937 staining of DNA with two dyes, dihydro-ethidium (DHE) and dsFLUOR. These dyes differ in
938 their affinities for kDNA vs. nuclear DNA, and measuring fluorescence in the Alexa Fluor 488
939 and Cy5-5 channels separates $kDNA^+$ and $kDNA^0$ populations. The representative image shows
940 the population before sorting for one of the induced replicates. Isolated $kDNA^0$ cells are then
941 scaled up by growing them for 80 hours in culture media before extraction of total DNA. (v)
942 RNAi fragments are PCR-amplified using RNAi cassette–specific primers. (vi) PCR amplicons
943 are then fragmented and Illumina sequenced. After mapping to the reference genome, the
944 number of mapped reads per gene is compared for the following samples: Comparison 1: day 5
945 +tet, sorted for $kDNA^0$ (n = 5) vs. uninduced day 0 (n = 5), unsorted. Comparison 2: day 5 +tet,
946 sorted for $kDNA^0$ vs. day 5 -tet, sorted for $kDNA^0$ (n = 5). (**B**) Establishing the FACS protocol
947 for differential staining of $kDNA^+$ and $kDNA^0$ cells. Images show the FACS plots from
948 optimized conditions using 1 µl dsFLUOR dye per 4 ml of cell suspension and 10 µg/ml
949 dihydroethidium. From left to right, cell populations are: control ($kDNA^+$) populations of kDNA-
950 independent *T. brucei*, the same cell line after treatment with ethidium bromide to remove kDNA
951 ($kDNA^0$), and a mix of these populations.

A

	1	2	3	4	5	6	7	8	9	10
1: CFAC1_040016200	100.00	65.48	40.50	41.19	41.04	21.95	22.60	22.16	23.80	22.17
2: LmjF.10.0810	65.48	100.00	42.06	42.19	41.92	19.95	21.57	23.42	23.97	21.98
3: TcBrA4_0019580	40.50	42.06	100.00	57.09	57.63	21.31	21.21	24.32	22.52	23.60
4: Tb927.8.4240	41.19	42.19	57.09	100.00	58.86	20.34	20.54	23.92	22.50	21.63
5: TvY486_0803620	41.04	41.92	57.63	58.86	100.00	22.01	22.03	24.57	23.41	22.65
6: CFAC1_040016100	21.95	19.95	21.31	20.34	22.01	100.00	48.07	33.40	30.54	32.48
7: LmjF.10.0800	22.60	21.57	21.21	20.54	22.03	48.07	100.00	32.38	30.36	31.18
8: TvY486_0803610	22.16	23.42	24.32	23.92	24.57	33.40	32.38	100.00	45.09	43.07
9: Tb927.8.4230	23.80	23.97	22.52	22.50	23.41	30.54	30.36	45.09	100.00	46.71
10: TcBrA4_0019600	22.17	21.98	23.60	21.63	22.65	32.48	31.18	43.07	46.71	100.00

B

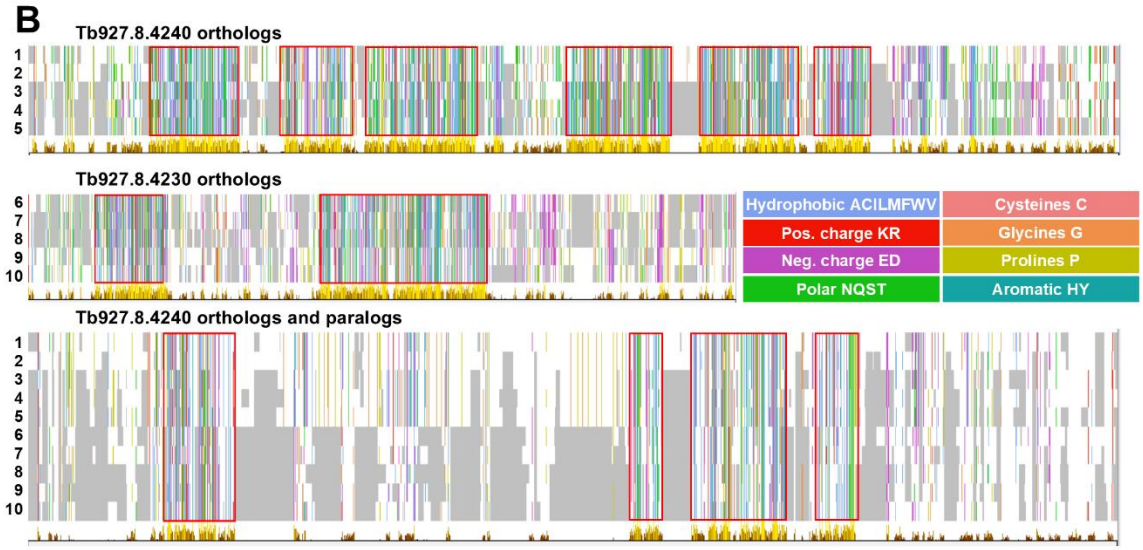

C

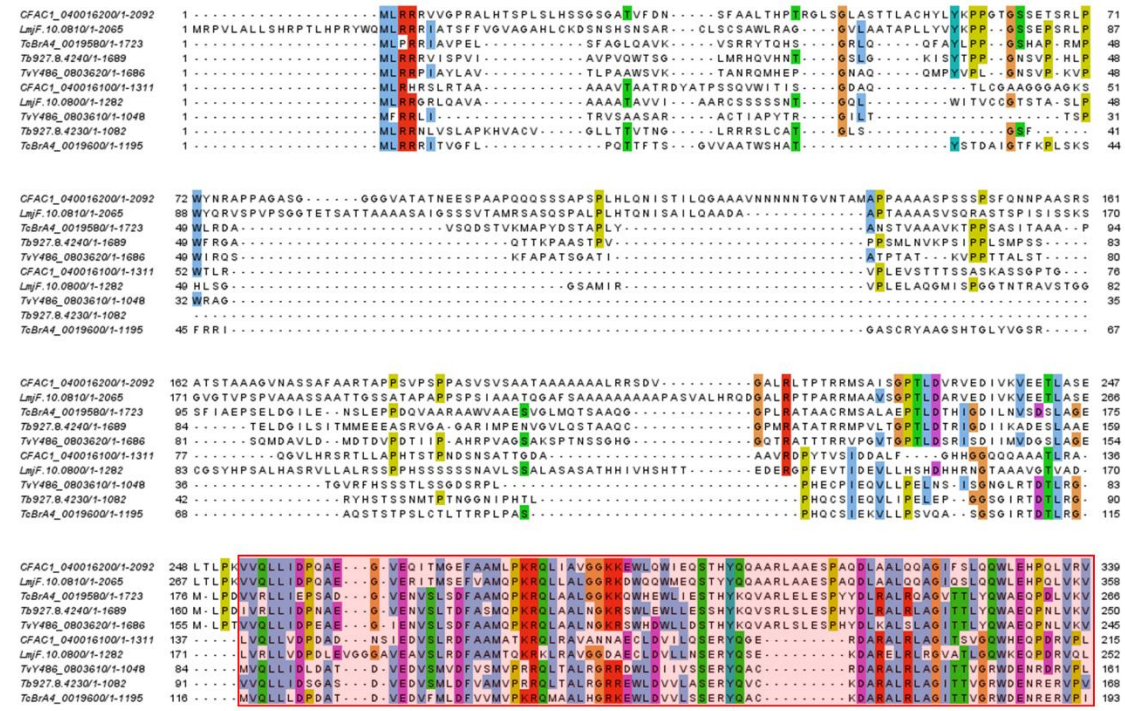

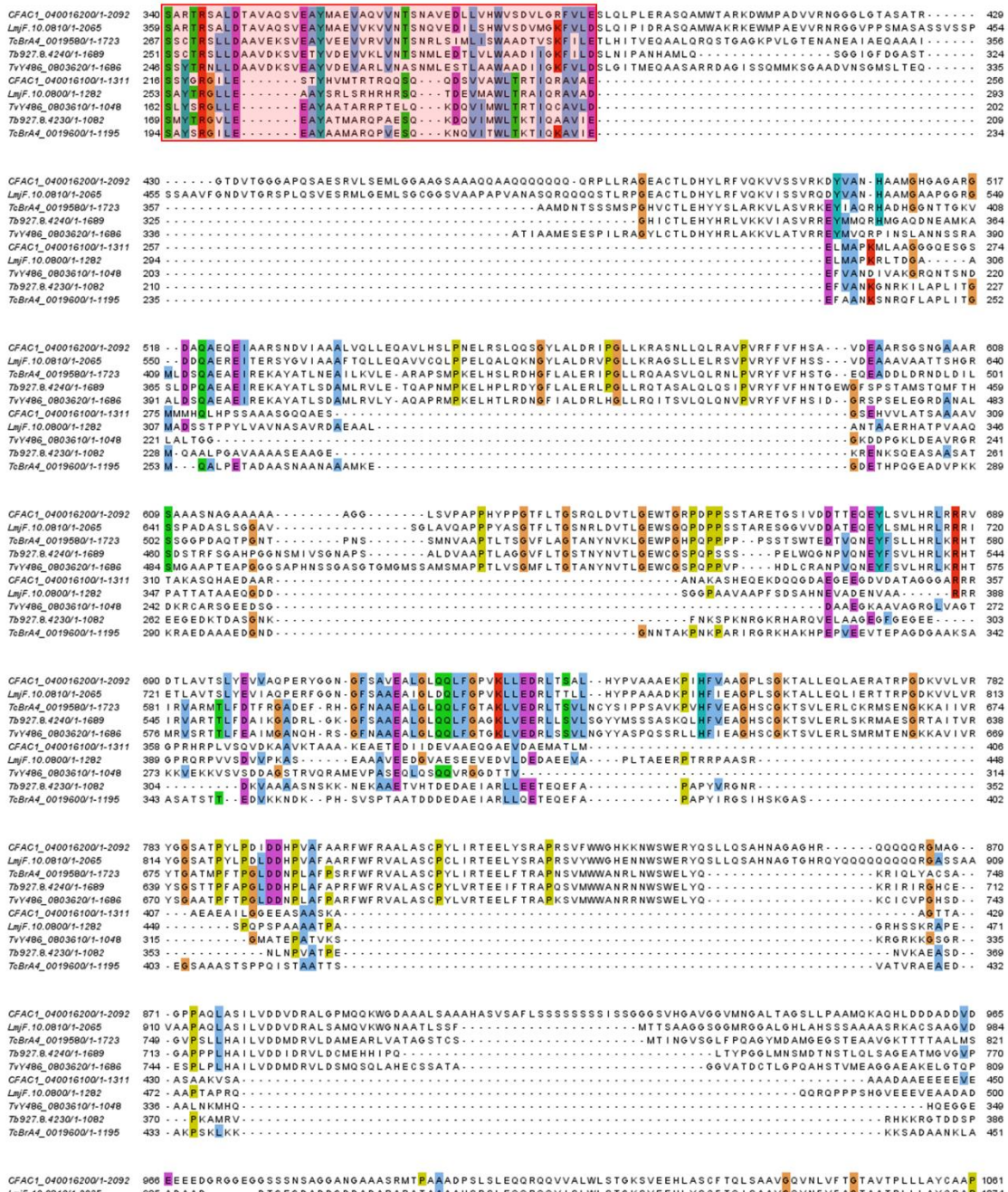
CFAC1_040016200/1-2092
LmjF.10.0810/1-2065
TcBrA4_0019580/1-1723
Tb927.8.4240/1-1689
TvY486_0803620/1-1686
CFAC1_040016100/1-1311
LmjF.10.0800/1-1282
TvY486_0803610/1-1048
Tb927.8.4230/1-1082
TcBrA4_0019600/1-1195

953

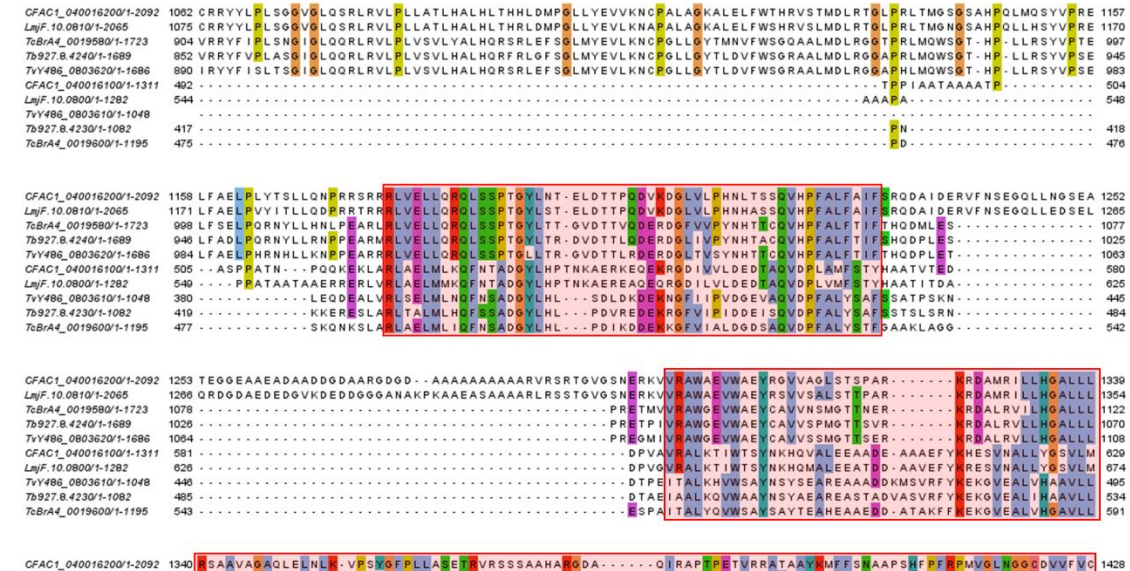
CFAC1_040016200/1-2092
LmjF.10.0810/1-2065
TcBrA4_0019580/1-1723
Tb927.8.4240/1-1689
TvY486_0803620/1-1686
CFAC1_040016100/1-1311
LmjF.10.0800/1-1282
TvY486_0803610/1-1048
Tb927.8.4230/1-1082
TcBrA4_0019600/1-1195

954

```
CFAC1_040016200/1-2092  1780 PSPQSLAPSLPQGAAAMAAAGGNTAAAAPQSRRAVPGRTAAEEAEADALAWLHDIISPESLIAGLKGTAPGAGTALANRASSASPSGVSAAAAPGQ 1875
LmjF.10.0810/1-2065     1777 PS------------IGASAADAAVTGVAPSKSSRAPGQTAADDAEADALAWLHDVITPESLIAGLKGSNPGAQVS-------APSSPSTATAAPGV 1853
TcBrA4_0019580/1-1723   1485 ------------------VAAGLLAARKTNSSSSSQPTTPGPAQEDALAWLHDIVTPATI------ATDGADG--------KLDQVTVRTTFSGN 1547
Tb927.8.4240/1-1689     1436 ------------------------------AVENTPHPAATASQEDALAWLHDIVTPAAA------SSQESDR--------SSATAPIAAYPSAS 1486
TvY486_0803620/1-1686   1484 ------------------------------MGPSTTSPPANAAQEDALAWLHDLITPAAV------SAPSTN---------PAGETSFRTTFSGE 1533
CFAC1_040016100/1-1311  1015 ----------------------TTRRTSAAAAAAPKGDEEEAELEEAIFSQWRKQKEQQ------QQQHGKHSV------SGGGGGSKSAAASR 1074
LmjF.10.0800/1-1282     1013 ------------------------------AAHAARDREQEEAMLEEAIYNQWQQQRGT-------SKAGAAAAT------TPKSMAVAQHSDND 1064
TvY486_0803610/1-1048    815 ------------------------------YEEEEEGEEEEEMEEEGEEESSAGSVPTAV------SFPAKKTSTPG----RGQSPKSHTSAAED  870
Tb927.8.4230/1-1082      857 ----------------------------EVEMADGEAVDEEEVKYEEVEEEQVNEQA--------EFHEAKK--------RPQQPLFASANGKR  906
TcBrA4_0019600/1-1195    947 --------------------------EEEEEEEDEEQKAGNGEEEDEEEEEEEAPREPPTI------SGNSRRHSLPAPV--KGRSARGRAHPAED 1008

CFAC1_040016200/1-2092  1876 QQSPQQQQQQAQQQSAAPPGNVGVGNFSAFAATAAAAGGGVMHPWTPN--VPAAAAADGT----ESIAAVFPRTAAKRDEAGRGDAPSAAPATEAS 1965
LmjF.10.0810/1-2065     1854 AASPQSPASPMAGMSLA-----AAGGGLASHASFAGSMASVTGPWTPNPIPPPVAASDGAGGERSSVAAGTPTTTTEEGERGAGAAAA-------- 1936
TcBrA4_0019580/1-1723   1548 PSSGAV---------------GSQAFVSLNNEEDVDVD-----------------------------------SNEEEEEEEEEEEE-------- 1584
Tb927.8.4240/1-1689     1487 TSRPAV----------------ITAPLPFNRKSNSSVTHSAMGNRATSTAREPAAELKK-------------VQEEVKRGKVSGQK-------- 1543
TvY486_0803620/1-1686   1534 MSRPQV----------------GTGSFVSLSNDEDVDGGAGEDEEGSF-----------------------LEDKMFDEEDEKES-------- 1579
CFAC1_040016100/1-1311  1075 AAAQQQEEEEEEGE---------EEEEFEEEEYEEEEAPVVTPAASKSRRGTASAAAASPASP---RAAAPRATTPAIEEEEEEEDEED-------- 1150
LmjF.10.0800/1-1282     1065 GASAEEAEEDFDE----------EYEEVEELEELEEAEKELPPARASARSSLPSASAAPGAGARARDAGASSPAPPASQAQGSSRAVAA-------- 1143
TvY486_0803610/1-1048    871 LSTKGTEEECGEG----------EEEEEEEEYEEEEVEEEVVTSRCMPAHASKKAVQPVRK-------------APQQTQQQEESMPRR-------- 936
Tb927.8.4230/1-1082      907 GGPPPTR----------------GREQRDRLQAMERGGDGVEGAPRRPSSQPDRKFVPDSF------------RSVPSSEIPPAPVPRR-------- 967
TcBrA4_0019600/1-1195    1009 AKKMREKDEEYDGE--------GDGDEPPRQHVQHVQQRAPPLRKTSHAGKRAPPPPPPA-------------ASGDDNDDDDDASD-------- 1074

CFAC1_040016200/1-2092  1966 GGDIDDDADVVEPEKTSSADDDGDADADAEEINLQKLFDAVSTNRRRSGRAT----------------SAATSSRQQRRGGATASGRRGSGTGSSS 2045
LmjF.10.0810/1-2065     1937 -GDVAETGESGDGEDDS-------GEGDEEELNAVKPRGAEGTRRKGGSKAGSKTTTVASRR------PRRESHSSNGKRSSAASRQKRSASMSRS 2018
TcBrA4_0019580/1-1723   1585 -GEGEEDEEAEDEEANH-------LGRQAVQPKGNKKSSNNGGTTRQRSRSQRSKSQKLKAKKLKNSPPSLSVARKKSGGNASSAAAAAAAAAAAA 1673
Tb927.8.4240/1-1689     1544 -IEVVEVEEVEVEEQSD----VEQATRDNKGRGRSRGRVSGSGSGSGTDGKGSSTKAVTGKRGRKPLQRSNVPEKKPKQQQANLKRTVQSVTPKRS 1634
TvY486_0803620/1-1686   1580 -VEILEEEEEHVVDERA-----KKSSDNDSGRQKPKKQAAKASSQSGGGKKG----------------AHSSASKKKSHQTSAASTSHASDTPR-- 1651
CFAC1_040016100/1-1311  1151 -VEIVKAPVLPRSPAGRRAVPVAQAVDDEEGVVDEEDEEELPPAPPRRAQQQQQQQRVARH----PQSSSAPAPTRPAQPPRAARVDEDVEEEDAP 1241
LmjF.10.0800/1-1282     1144 -VDAAAADEEEYEEDSV--------EEEEEEAEEMEVVTAPTIPRAPAGRRA-------------VPVAAAPARPSPPPPPPSPAVRRAPQKLDDD 1217
TvY486_0803610/1-1048    937 -GQIVRKRAPVVEEKHY---------DDEQEEEQEEEEEEEEEVVRPPVKK----------------SLPLRRATSSPLRSGAGAREEYEDDEAE 1004
Tb927.8.4230/1-1082      968 -GYITRRPAPPVMNHEV-----DEIEEEEEEAVRRPIRRTPPTRRPPSPSFQ-------------SSPQPSPSRLQGDAAVREVSYDDEEAEA 1041
TcBrA4_0019600/1-1195    1075 -ADDNKEEEVHAQPQSQ-----QHTAVSKKGHATKKSPPPPPTTATTDNDEDEEEEEVVRR-----PTKKGVSSKRAPPPPVAAQNDDSKEEEEEV 1159

CFAC1_040016200/1-2092  2046 GSSSSAKAKAKGKKAGGGASSSASKSK-------------------AKVSAASGGKKKASAAKKKK--------                          2092
LmjF.10.0810/1-2065     2019 DDRATARSAPQSTSQTKRRKPLTSKKN-------------------QAAPSSSSSRKKKSNSSRRR--------                          2065
TcBrA4_0019580/1-1723   1674 TAAAAESAAAAQARRKGGKLKKRSSKT-------------------VPSSPSRSAAAAGGEKKRKKKKR-----                          1723
Tb927.8.4240/1-1689     1635 SSSSSTTAASSRGRNKSRELAKPAKRT-------------------TSRASVAAASKTDKNAKKKQKKSALRMV                          1689
TvY486_0803620/1-1686   1652 -------------GKRAQGRGAKADKRT-------------------TAATVASEAAKTKKAAKKKK--------                          1686
CFAC1_040016100/1-1311  1242 PPLPLIRTRRGAARRHSSRAPVAPQTEETGEESASAGLSGEDGAEGSEGAPVAAAEDQWFRKKPKRRYFE----                          1311
LmjF.10.0800/1-1282     1218 DEALQVRTRRGARRSTARARAPPPTAHEDFEEAAAAAVEGA-----PEVAAEDADEDQWFKKRPKRRYFQ----                          1282
TvY486_0803610/1-1048   1005 EVAPRPRVRPGGNVVTNRRVGRPPSQS-------------------SPSSLGVGDKERWFDRR----------                          1048
Tb927.8.4230/1-1082     1042 ELTTRPRVRSTSGVRRVGRVAISNSSD-----------------------IIGDEDRWFERVRR--------                          1082
TcBrA4_0019600/1-1195   1160 VVAPRVRNR---GRRMSRALPQSSSDS-----------------------NDEDRWFQRARR--------                          1195
```

956 **Fig S2** Sequence conservation of *Tb*927.8.4240 protein orthologs and paralogs in selected
957 trypanosomatids. Sequences 1-5: *Tb*927.8.4240 orthologs. Sequences 6-10: Tb927.8.4230
958 orthologs. 1, 6: *Crithidia fasciculata* (Cf-C1). 2, 7: *L. major* (Friedlin). 3, 8: *T. cruzi* (Brazil A4).
959 4, 9: *T. b. brucei* (TREU 927). 5, 10: *T. vivax* (Y486). (**A**) Percent identity matrix, generated
960 using Clustal 2.1. (**B**) Overviews of sequence conservation in *Tb*927.8.4240 orthologs (top
961 panel), *Tb*927.8.4230 orthologs (middle panel) and *Tb*927.8.4240 orthologs and paralogs
962 combined. Alignments were generated using Muscle
963 (https://www.ebi.ac.uk/jdispatcher/msa/muscle) (98) and visualized using Jalview (99). Amino
964 acids are colored according to the Clustal color scheme in Jalview. Each residue in the alignment
965 is assigned a color if the amino acid profile of the alignment at that position meets some
966 minimum criteria specific for the residue type (40% identity threshold). Blue: hydrophobic (A,
967 C, I, L, M, F, W, V). Red: positive charge (K, R). Magenta: negative charge (E, D). Green: polar
968 (N, Q, S, T). Pink: cysteines (C). Orange: glycines (G). Yellow: prolines (P). Cyan: aromatic (H,
969 Y). White: unconserved. A track with bars underneath the individual sequences reflects the
970 conservation of the physico-chemical properties for each column of the alignment, calculated
971 based on the AMAS method of multiple sequence alignment analysis (100). The higher the
972 score, the taller the bar and the lighter the shading (highest scores being reflected by yellow). (**C**)
973 Detailed sequence alignment of selected Tb927.8.4240 orthologs and paralogs. Sequences and
974 color codes are as in panels A and B. Red boxes and shading indicate regions of relatively high
975 conservation.

976

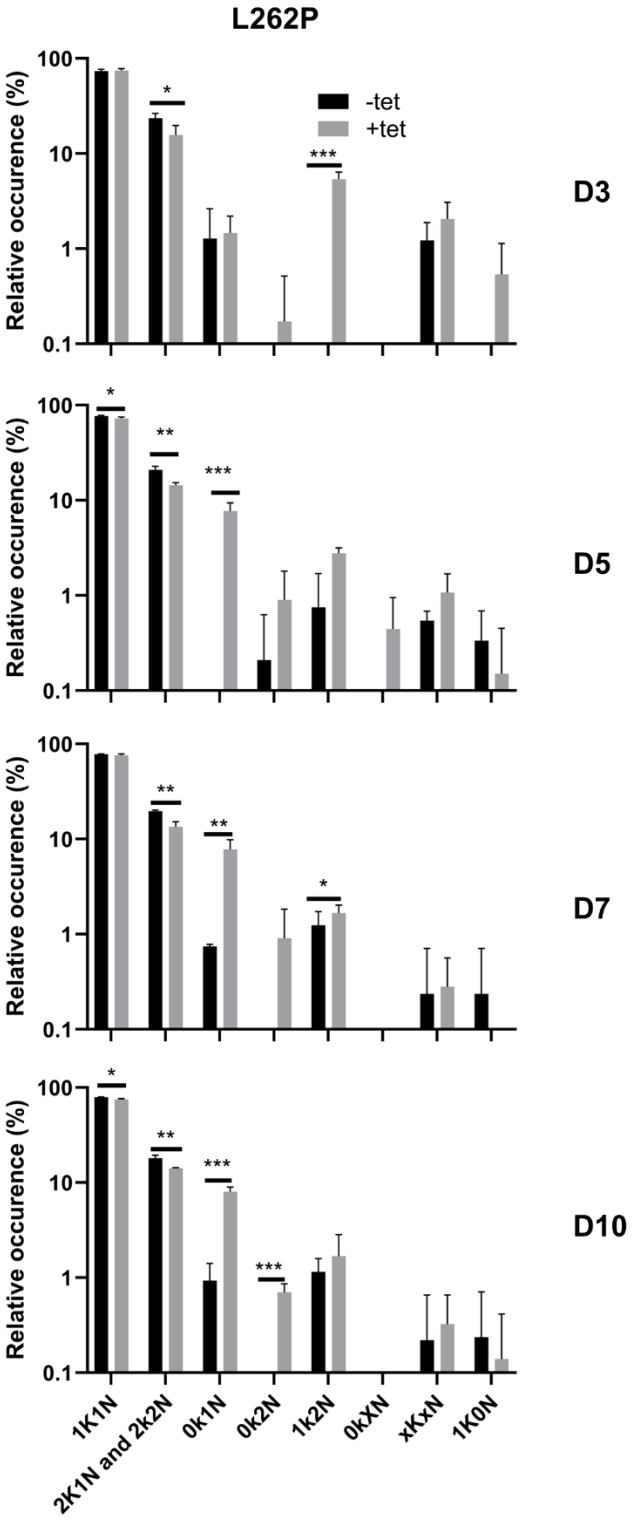
L262P
-tet
+tet
Relative occurence (%)
100
10
1
0.1
D3
D5
D7
D10
1K1N
2K1N and 2k2N
0k1N
0k2N
1k2N
0kXN
xKxN
1K0N

977

978 **Fig S3** Quantification of relative occurrence of kDNA (K) and nuclei (N) in DAPI stained cells
979 from induced (+tet) and non-induced (-tet) Tb927.8.4240 RNAi cells in the kDNA-independent
980 γL262P background. Data for days 3, 5, 7 and 10 post-induction are shown (n>100 cells for each
981 triplicate; unpaired t-test P<0.05*, <0.01**, <0.001***).